

Biogeosciences Discuss., 11, C6235–C6238, 2014  
www.biogeosciences-discuss.net/11/C6235/2014/  
© Author(s) 2014. This work is distributed under  
the Creative Commons Attribute 3.0 License.

***Interactive comment on “Chemometric perspectives on plankton community responses to natural iron fertilization over and downstream of the Kerguelen Plateau in the Southern Ocean” by T. W. Trull et al.***

**Anonymous Referee #1**

Received and published: 27 October 2014

This is overall a very interesting and informative manuscript (MS), as one of the many contributions from the KEOPS2 expedition. In the MS, the surveyed area over and downstream of the Kerguelen Plateau was clustered into 5 groups based on ocean circulation patterns and characteristics of natural iron fertilization. For each group, a wide range of original data, including POC, BSi/POC,  $\delta^{13}\text{C}$ , and  $\delta^{15}\text{N}$ , were measured for various plankton size groups. These measurements were further used as proxies to estimate size-specific biomass, fraction of diatoms, growth rate, and f-ratio, respectively. The authors also calculated the N and Si depletion in the water column and estimated export production based on these calculations. Setting these data in the context of the whole KEOPS2 study, the authors gave a detailed picture of the different responses of the plankton community to various types of natural iron fertilization, namely, the punctual and high level vs. the persistent yet relatively low iron supply, and came to several interesting points, e.g., the carbon export was decoupled from surface biomass, and the export could be higher in areas with low but lasting iron supply relative to areas with high but punctual supply.

The authors showed innovative utilization of several chemical proxies (although some of them have very large uncertainties), and discussed in great depth about the relationship between iron fertilization and carbon export. I would recommend this MS for publication on Biogeosciences, after the following comments are addressed, and a thorough proofreading is done.

Comments:

1. One interesting point the authors made is that the carbon export in the area with long-lasting but low iron supply may exceed that in area with episodic and strong iron supply. I would like to see a clearer definition of the time window of the carbon export the authors are examining and comparing. It seems that accumulation of biomass and export reported in the Polar Front Plume region represent an early phase of the iron-induced phytoplankton bloom, with a large standing stock of biomass in the mixed layer waiting to be exported, while the water in the recirculation feature has experience one or several full cycle(s) of phytoplankton growth and export. Considering the lag of export after the bloom, would export in the Polar Front region be much higher, and the conclusion be very different, if the experiment were extended for one more month?

**AUTHOR RESPONSE**

We agree with the reviewer that it is not possible to know the subsequent evolution of export over the seasonal cycle, but it is possible that this would change the perspectives that apply for our observed spring period. We added text to explicitly recognize this, in the Results section 3.5:

**MODIFIED TEXT**

Of course observation of these variations in spring does not mean that they would have persisted into summer, and it is possible that over the full season the extent of nutrient depletion was significantly different, either towards homogeneity across the region or towards larger variations.

Is it possible to define a term T that is the days from the initiation of phytoplankton blooms to the day of sampling for each of the 5 groups, and compare the export in the unit of  $\text{mmol m}^{-2} \text{ day}^{-1}$ ?

**AUTHOR RESPONSE** We provided two time metrics in the text: “time since

fertilization” and “time since biomass accumulation” but both of these can only be estimated very approximately (at best two within a few weeks), and neither provides information on when export actually began, so we prefer to make the comparisons in the context of these approximate time frames in the text and not to provide false quantification. To make the times more clear we now list both of them in a revised version of Table 1:

2. The integration depth of the Group 5 (downstream PF plumes) stations based on the S-threshold method is overall significantly smaller than other stations. The choice of the S-threshold method over the T-min method thus accounts largely for the conclusion that the export in the Polar Front plume area was smaller than that in the recirculation area. It is possible that the authors are comparing water columns without much stratification since winter mixing to water columns that have recently being stratified and shoaled? A fuller description regarding the evolution of the hydrological structure would be very helpful.

**AUTHOR RESPONSE** The reviewer is correct that the choice of depth for the nutrient depletion estimate has a very strong influence, in particular for these sites at the Polar Front which show salinity stratification above the depth of the winter-derived temperature minimum. And this is exactly why the Tmin depth should not be used, because stratification by horizontal mixing has re-defined the stratification and nutrient profiles between the two depths (Tmin and Sthreshold) more recently than the end of winter. Because the high biomass layer found in these Polar Frontal sites is in this shallow salinity-defined layer, and because the Fe fertilization of these waters is recent as shown by their short transit time since crossing the plateau (because the flow along the Polar Front is fast as determined from both altimetry and drifter releases (d’Ovidio et al., 2014; Park et al., 2014). We have added information on this to the text in section 3.5:

**MODIFIED TEX** We believe the  $S_{\text{threshold}}$  approach is the most appropriate given the observed salinity stratification, especially for the relatively weak subsurface thermal stratification observed in the Group 5 stations near the Polar Front, where it’s choice makes the most significant difference from estimates based on the  $T_{\text{min}}$  approach. This is because the high biomass layer found in these Polar Frontal sites is in this shallow salinity-defined layer, and because the Fe fertilization of these waters is recent as shown by their short transit time of ~ 2 weeks since crossing the plateau as determined from both altimetry and drifter releases (d’Ovidio et al., 2014; Park et al., 2014). Thus attribution of nutrient depletion below the depth of the  $S_{\text{threshold}}$  to iron fertilized biomass production is not warranted.

3. The authors talked at several points in the MS about the influence of lateral transports on the calculated f-ratio and export production. Considering that the influence of lateral transport may be very different in the Polar Front Plume and the recirculation area, a more quantitative description about the lateral transports (e.g., timing, current in m/s) will be very helpful .

**AUTHOR RESPONSE** We agree that this information is important, and we have summarized it in the context description in Methods Sections 2.1 and 2.2, provided an overview of the timing in Table 1, and included an animation of the biomass transport in the supplementary materials with a running calendar. Because the transport pathways are complex, time-varying, and their understanding requires detailed figures and discussion, it is best to refer readers to the sources of this information in the papers by Park et al., 2014 and d’Ovidio et al., 2014, as we have done in both these Methods sections and in the Results section 3.5. .

4. In the discussion (section 4.1), the authors reported that the growth rate calculated from the d13C measurements is higher in G4, then G3 and G5 and then G1 and G2. However, there does not seem to be significant difference between G1, G2, G3 and G5 on Figure 5. In addition, it seems that the model results, compared with the 13C uptake results, tend to over-estimate the growth rate by a factor of 2. Can the authors provided a little more discussion about the uncertainty of the d13C isotopic fractionation model method, e.g. , a sensitivity test on the growth rate derived from different assumptions about the cell shape and dimensions?

**AUTHOR RESPONSE** We agree with the reviewer that this issue was insufficiently addressed and we have added several sections of new text that describe the large uncertainties in our calculated growth rates and emphasize that the overall conclusions do not rely upon them alone. For the full details, please see our extended response to Reviewer2 on this issue, which includes these new sections of text.

There are some minor issues the authors may need to consider:

1. It is probably more proper to move Section 2.2 and 2.3 to the Chapter 3 (Results)

s they are reporting actual data in great details;

**AUTHOR RESPONSE** Because this results come from other papers, as cited, we prefer to keep them in the Methods section along with all the other information on oceanographic context.

2. Line 27, pg. 13847: what is the difference between A3-1 and A3-2?

We added text to explain that these names reflect two visits to the same site.

3. Line 26, pg. 13850: do you mean “plateau<= Polar Front plume”?

**AUTHOR RESPONSE** Yes, thank you, and we corrected this typo as suggested.

5. Line 24, pg. 13857: Missing digit after “8.”?

**AUTHOR RESPONSE** Yes, thank you, and we corrected this typo to show the full value of 8.0.

6. Line 18, pg 13861: what does the  $^{13}\text{C}$ -POCs mean for the heterotrophic dominated size fractions?

**AUTHOR RESPONSE** Heterotrophs tend to have  $^{13}\text{C}$ -POC values similar to their prey, with additional contributions from low  $^{13}\text{C}$  lipid reserves for organisms that form them. We added text as follows:

**MODIFIED TEXT** The presence of lipid-rich zooplankton in the two largest size fractions is another probable cause of their low  $^{13}\text{C}$ -POC values, based on low  $^{13}\text{C}$ -POC values for zooplankton collected with nets during KEOPS2 (Carlotti, 2014).

7. Figure 1. a) Latitude and Longitude on the left-bottom corner of the figure is not very readable. Could you put the numbers out of the box? b). Is it possible to show the location of the Station R on this figure?

**AUTHOR RESPONSE** We made both changes as requested.

8. Figure 2. Kerguelen and Heart Island on this map are not very distinguishable from the clouds. Is it possible to mark the islands using darker color?

**AUTHOR RESPONSE** We made this improvement as requested.

8. Figure 3. The x-axis in the middle panel is log(size), while on other figures it shows “filter size”. It seems to be more straightforward to use “filter size”.

**AUTHOR RESPONSE** We made this improvement as requested.

Interactive comment on Biogeosciences Discuss., 11, 13841, 2014.

## Anonymous Referee #2

Received and published: 3 November 2014

In this manuscript results from the KEOPS2 survey in the vicinity of the Kerguelen Islands are presented. The purpose of the study is the understanding of the impact of natural iron fertilization on productivity and biogeochemistry of the Southern Ocean. These studies are highly relevant to our understanding of the impact of changes in the SO biological pump on past (Glacial/Interglacial) and future atmospheric pCO<sub>2</sub>. Here results on the size-fractionated composition of particulate organic matter (BSi, POC, PON,  $\delta^{13}\text{C}$  and  $\delta^{15}\text{N}$ ) as well as estimates on nutrient utilization and, by comparison with standing stocks, export are presented. Further,  $\delta^{13}\text{C}$  and  $\delta^{15}\text{N}$  of particulate size fractionated organic matter is used to estimate growth rates and f-ratios of the different size classes in the community. Results are interpreted to infer the impact of different intensities in iron fertilization (based on hydrography and location) on community structure, and the impact of community structure on biogeochemistry.

I commend the authors on their effort to interpret the data, but must confess that I am not too convinced by the manuscript. Most of the data interpretation is based on indirect evidence itself based on assumptions that are possibly not valid (see also comments below).

## AUTHOR RESPONSE

We consider that this statement is a fair assessment for one of our chemometric methods (growth rates estimated from  $^{13}\text{C}$ , for which we provide further discussion below and have added a large section of new text regarding the associated caveats in the paper), but not for the others. Specifically, our measurements of the size distribution of POC, PN, and BSi do provide direct quantification of some of the most important characteristics of pelagic microbial ecosystems: i) size structure, which more than 50 years of measurements and models has placed at the centre of the understanding of ecosystem function, ii) the possibility of the presence of significant levels of detritus with higher C/N than autotrophs (not strongly present in this case), and iii) the extent of nitrogen recycling as estimated from the  $^{15}\text{N}$  natural abundance contents of the community (this can be argued to be indirect, but neither reviewer raised any specific objections to this approach and in this paper and in previous work over the Kerguelen plateau (Trull et al., 2008) we have shown excellent correlation with the more time-consuming  $^{15}\text{N}$ -tracer incubation approach to determining f-ratios). Nutrient depletion methods are also well tested to estimate export, especially in the Southern Ocean where the presence of the winter mixing derived temperature minimum provides a good guide to the initial water column inventory (see references in Sweeney et al., 2000). Yes, we also examined a salinity based estimate of the winter inventory, which is more uncertain (and we have added further discussion of this uncertainty in the revised paper), but we did not do this lightly and we do cite careful previous assessments of the scope of the probable biases from this approach (up to 2x, but more typically 30%, Wang et al., 2003).

Further, there are better and more direct methods to study both community composition and export.

## AUTHOR RESPONSE

We agree that community composition is most directly and precisely studied by microscopy, and that other methods such as pigment analyses can also, in some cases, be more powerful than size-fractionated bulk chemical measurements (although we note with irony that the main use of pigment analyses from the KEOPS1 experiment was to estimate the size structure of the community, in keeping with the importance of size in assessing ecosystem function, Uitz et al., 2009). Microscopic study and pigment analyses were also pursued during KEOPS2, and we have cited the components of that work that are available (Lasbleiz et al, 2014 and L. Armand personal communication). But we don't agree that this knowledge necessarily makes it any easier to quantitatively connect community composition to export, because conversion of biovolumes to units of elemental concentrations for biomass quantification (and its subsequent comparison to dissolved nutrient fields) also has large uncertainties. Direct measures of export using free-drifting and gel-filled sediment traps were also carried out during KEOPS2, with this effort led by lead author Trull and published by his PhD student Laurenceau (Laurenceau et al., 2014). But this time consuming method could only be carried out at 6 sites (whereas our work examined 33) and has its own large uncertainties regarding trap collection efficiencies. In summary, and as is well known, evaluating ecosystem controls on export requires the application of multiple methods, (as many as possible!), and we have provided a large suite in this paper, and also cite and discuss many others from additional papers in this special volume, including the indirect method of  $^{234}\text{Th}$  inventories.

Although I concur with the main conclusions of the study (i.e. high biomass and productivity does not necessarily lead to high export and is dependent on the community composition), this is already well known and the use of bulk parameters (as presented here) adds little to our understanding.

#### AUTHOR RESPONSE

In a broad sense we agree that this is well known, but we think that understanding this under the mesoscale varying conditions of iron fertilization in the Southern Ocean is far from resolved. For example, the high biomass over the Kerguelen plateau does correlate well with enhanced carbon export (both in autumn and for the full season, Blain et al, 2007; Jouandet et al., 2008; Ebersbach and Trull, 2008). But here we show that this does not necessarily extend to the downstream plume, and that this is not necessarily true in springtime. .

Finally, when studying export (highly dependent not only on whole community but possibly on behavior of individual species), there is a temporal component not taken into account (i.e. most of the export does generally not occur during the growth phase of a bloom) and is possibly masked by the large spatial variations in the area of study.

#### AUTHOR RESPONSE

Yes, we agree, and we addressed these temporal and spatial aspects in great detail by providing i) a full annual animation of the bloom development as seen by satellite surface Chla image, ii) 4 images detailing the stages of the bloom at the times of shipboard sampling, iii) two temporal metrics: time since Fe fertilization and time since onset of surface Chla accumulation. We suspect the reviewer means to imply that our assessment of spatial variations may not hold over the whole season, and of course that is true and we have added text to make this very explicit in the revised version in section 3.5:

#### MODIFIED TEXT

Of course observation of these variations in spring does not mean that they would have persisted into summer, and it is possible that over the full season the extent of nutrient depletion was significantly different, either towards homogeneity across the region or towards larger variations.

#### AUTHOR RESPONSE

[As an aside, we do not agree with the reviewers statement that “most of the export does generally not occur during the growth phase of a bloom”. Our view is that most of the time ~90% of the production is removed by grazing (with a component of this sinking as fecal pellets each day) or aggregate sinking, and that even during the rapid build up of biomass at the start of a bloom this probably only drops to ~50% (indeed for our case this is the approximate value suggested by this reviewer in the last paragraph below) and thus at best the accumulation of biomass during the bloom might represent half the total seasonal export if it is all exported in autumn. This perspective of the autumn export being important but not dominant is consistent with results from the vast majority of deep ocean sediment trap time series (e.g. the reviews of Lampitt and Antia, 1997 and Lutz et al, 2007)]. .

As the paper seems somewhat to be an attempt at synthesising results from the whole study, I would recommend the authors incorporate in their results and discussion other measurements (submitted in separate papers in this issue) in a more explicit manner.

#### AUTHOR RESPONSE

Our paper is focused on the chemometric results, which (as both reviewers have requested), requires detailed explanation of their uncertainties and their implications, and thus is not the right place for a broader synthesis (although we do cite and discuss comparisons to many other results from KEOPS2).

#### Additional comments:

Lines 311-318: In the description of the community how were non-diatom protists (including heterotrophs important in the < 210µm size fractions) assessed? These tend to be more delicate and probably damaged during filtration.

#### AUTHOR RESPONSE

We added text as follows:

#### MODIFIED TEXT

These microscopic assessments of the materials present on the filters are rather limited, and may well have missed significant contributions from autotrophs and heterotrophs without frustules or carapaces, but other studies during KEOPS2 of bacterial abundances (Christaki et al., 2014), phytoplankton (Georges et al., 2014; Lasbleiz et al., 2014), diatom species (L. Armand, personal communication), and zooplankton (Carlotti, 2014) are consistent with our chemometric interpretation that detritus, bacteria, and phytoplankton contributed to the 1 um fraction; phytoplankton and especially diatoms dominated the 5, 20, and 50 um fractions; a mix of large diatoms and copepods were present in the 210 um fraction and copepods, isopods, and occasionally krill were the primary contributions to the 300 um fraction.

Growth rates estimates from  $\delta^{13}\text{C}$  of POC are based on the assumption that cells do not use bicarbonate. From previous laboratory studies, bicarbonate use is common and highly variable at a species-specific level (also dependent on light regime). I am not sure that any of the growth rates estimates given here are reliable. Also the authors failed to refer to the studies on this topic: Burkhardt et al. (1999) *Geochimica et Cosmochimica Acta*, 63: 3729-3741, Burkhardt et al. (1999) *Marine Ecology Progress Series*, 184: 31-41; Rost et al. (2002) *Limnology and Oceanography*, 47(1): 120-128. I also fail to see large differences in growth rate estimates for the different groups (Fig. 5).

#### AUTHOR RESPONSE

We share the reviewers' concerns regarding the fidelity of our transformation of the  $^{13}\text{C}$ -POC values into growth rates (and not only because of the issue of  $\text{CO}_2$  versus bicarbonate use), and we acknowledge that our introduction to the associated issues and uncertainties was too brief. We have completely rewritten the introduction to this section to cite these and many other works and to provide a clearer explanation of the influences of bicarbonate and  $\text{CO}_2$  uptake. In this regard, we note that while the Popp et al (1998) model fit to observed  $^{13}\text{C}$  dependencies on growth rate did assume uptake was solely of  $\text{CO}_2$ , this assumption is not necessary (as shown by the modeling work of Keller and Morel, 1999).

#### MODIFIED TEXT

Controls on the  $^{13}\text{C}$  composition of phytoplankton are complex, and have been explored in hundreds of papers since an early survey of the variability in marine carbon isotopic compositions (Craig, 1953), with occasional significant advances and reviews, e.g. (Farquhar et al., 1982; Goericke et al., 1994; Laws et al., 1995; Laws et al., 2002; Rau et al., 1996; Schulz et al., 2007; Tortell et al., 2008). In brief, there are two main causes for  $^{13}\text{C}$  variations of any given phytoplankton cell. Firstly, the cell  $^{13}\text{C}$  content depends on the chemical form of DIC that is assimilated, because the less abundant aqueous molecular  $\text{CO}_2$  form contains much less  $^{13}\text{C}$  than the bicarbonate anion form which makes up more than 90% of the total DIC. At the temperatures pertaining during the KEOPS study, this equilibrium fractionation lowers the  $^{13}\text{C}$  content of aqueous molecular  $\text{CO}_2$  by ~11‰ (Rau et al., 1997):

$$^{13}\text{C-CO}_2 = ^{13}\text{C-DIC} + 23.644 - 9701.5/T_{\text{kelvin}} \quad (1)$$

Secondly, the cell  $^{13}\text{C}$ -POC content depends on the extent to which the enzymatic kinetic discrimination against  $^{13}\text{C}$  during photosynthetic carbon fixation (of 20-30 ‰, varying with the specific metabolic pathways) is expressed. It is only fully expressed when inorganic carbon flow into and out of the cell (supply) is faster than fixation (demand).

Both these effects often lead to higher  $^{13}\text{C}$  contents in faster growing cells, because faster growth favours use of the more abundant bicarbonate form of DIC and also leads to less expression of the kinetic fractionation. Thus the association of higher  $^{13}\text{C}$  contents with faster growing cells is very strongly justified for any particular phytoplankton species, from both metabolic understanding and the plethora of batch and chemostat experimental studies. Despite this understanding, inferring growth rates for communities of phytoplankton from field measurements of  $^{13}\text{C}$ -POC is fraught with difficulties. The magnitudes of these two main isotopic effects vary strongly among different phytoplankton (and with their conditions of growth including temperature, nutrient and trace metal availability, light levels, specific enzymatic pathways, etc. (Burkhardt et al., 1999b; Burkhardt et al., 1999c; Fontugne et al., 1991; Schulz et al., 2007)), and there is no universal quantitative relationship between growth rate and phytoplankton  $^{13}\text{C}$  content. In particular, cell size is a key variable in the control of  $^{13}\text{C}$  contents (Popp et al., 1999; Rau et al., 1996; Rau et al., 1997; Rau et al., 1990), and the global range of surface water  $^{13}\text{C}$ -POC values can be observed within a single Southern Ocean sample, simply via its size fractionation (Trull and Armand, 2001). Good correlations between growth rates and  $^{13}\text{C}$  contents when cell size is expressed in terms of the surface/volume ratio suggest this results from the balance of supply versus demand (Popp et al., 1998b), of either or both aqueous  $\text{CO}_2$  and bicarbonate forms (Burkhardt et al., 1999a; Keller and Morel, 1999; Schulz et al., 2007), and with further

Formatted: Font: (Default) Times New Roman, 9 pt, Font color: Light Blue, Not Highlight

modulation by other environmental controls such as the availability of light and other nutrients (Burkhardt et al., 1999c; Gervais and Riebesell, 2001; Schulz et al., 2004).

This complexity means that our observed  $^{13}\text{C}$ -POC variations, even within a given size fraction, could arise by multiple mechanisms. Higher  $^{13}\text{C}$  contents could reflect faster growth rates (via either greater use of bicarbonate or an increase of fixation of all DIC chemical forms relative to supply), or might instead reflect changes in species with inherently different uptake and assimilation metabolisms, or changes in metabolism driven by other controls such as light or iron availability. Our chemometric methods cannot distinguish among these possible causes, and thus our expression of the  $^{13}\text{C}$ -POC variations in terms of growth rate variations can only be viewed as an indicative exercise. To pursue this, we chose a model fit to chemostat data (Popp et al., 1998b);

$$^{13}\text{C-POC} = (^{13}\text{C}_{\text{source}} - \epsilon_p) + k \text{ demand-rate/supply-rate} \quad (2)$$

in which the first term expresses the lowest possible  $^{13}\text{C}$  contents of the cell as growth rate approaches zero, and the second term describes the linear (constant k) dependence of isotopic composition on the relative rates of  $\text{CO}_2$  supply into the cell and its cellular fixation. Popp et al. (1998) assumed the chemical form was aqueous molecular  $\text{CO}_2$  but further evaluation showed that the data could also be fit by a model allowing either or both  $\text{CO}_2$  and bicarbonate uptake (Keller and Morel, 1999). Both models assume that the, supply rate depends linearly on its external concentration modulated by the surface area of the cell, and thus while the fitting constants we use here are from Popp et al (1998), the scaling to the surface/volume ratio (S/V) of the cell is independent of the chemical form of uptake);

$$^{13}\text{C-POC} = (^{13}\text{C-CO}_2 - 25) + 182 \mu / ([\text{CO}_2] \text{S/V}) \quad (3)$$

Rewriting this equation for growth rate,  $\mu$ , and our measured  $^{13}\text{C}$ -DIC and  $^{13}\text{C}$ -POC values yields an indicative path to possible growth rates for our size fractions:

$$\mu = \text{S/V} [\text{CO}_2] [^{13}\text{C-POC} - (^{13}\text{C-CO}_2 - 25)] / 182 \quad (4)$$

with  $^{13}\text{C-CO}_2$  calculated using equation (1),  $[\text{CO}_2]$  obtained from underway  $\text{pCO}_2$  observations (Lo Monaco et al., 2014) and Henry's Law (Weiss, 1974). In this expression, growth rate  $\mu$  is in  $\text{d}^{-1}$ , S/V in  $\mu\text{m}^{-1}$ , and  $[\text{CO}_2]$  in  $\mu\text{mol kg}^{-1}$ .

This expression provides growth rates that we compare to other estimates. Of course, comparison of these rates is very sensitive to S/V estimates, as well as to all the other possible sources of variations in  $^{13}\text{C}$  contents summarized above. For example, a 30% increase in the mean size of cells, such as could occur within a given size fraction, would yield a 69% increase in the model growth rate (for spherical cells). For this reason, our growth rate estimates must be viewed with great caution, not only in terms of their absolute magnitudes, but also in terms of their relative magnitudes across the different stations.

#### AUTHOR RESPONSE

In addition to this revised text regarding our growth rate estimates we have added caveats at several places in the Results and Discussion sections to emphasize that the growth rates are not quantitative and that our conclusions are not based solely upon them:  
New text in Results Section 3.3:

#### MODIFIED TEXT

This provides a useful cautionary note that the apparent growth rate variations have no real quantitative validity; at best they provide indicative information on the relative intensities of  $\text{CO}_2$  assimilation across the Groups. Indeed, it is possible that the variations among the Groups results from other issues such as species metabolic differences, or light and trace element availability (as discussed in detail in the Methods section). Thus it is important to emphasize that the overall view of ecosystem responses developed in the Discussion section does not depend only on these potential growth rate estimates from the  $^{13}\text{C}$ -POC observations, but also draws on biomass accumulation rates from the POC concentrations, their distribution across size fractions, and other indicators as discussed below.

#### AUTHOR RESPONSE

New text in Discussion Section 4.1.:

#### MODIFIED TEXT

Both of the more strongly iron fertilised offshore regions (the Group 3 central plateau and the Group 5 Polar Front bloom, Table 1.) exhibited increased  $^{13}\text{C}$  model growth rates in comparison to HNLC waters (elevated by  $\sim 0.05 \text{ d}^{-1}$ ), but their community structures were quite different (emphasizing caution regarding the  $^{13}\text{C}$  model growth rates, although the incubation results also indicated increased growth rates; (Cavagna et al., 2014)).

I am not sure of the logic in separating some of the stations in 2 groups (groups 1 and

Formatted: Font: (Default) Times New Roman, 9 pt, Font color: Light Blue, Superscript

Formatted: Font: (Default) Times New Roman, 9 pt, Font color: Light Blue, Superscript

Formatted: Font: (Default) Times New Roman, 9 pt, Font color: Light Blue, Superscript



2) as they are in a similar location and could be used to infer temporal development.

#### AUTHOR RESPONSE

This was done largely for convenience to have a manageable number of stations in each of these two groups, and the temporal aspect is discussed in just the way the reviewer recommends – as an evolution from the status observed in Group 1 towards that observed in Group 2, and then with additional consideration of the temporal evolution within Group 2 which was specifically carried out as a time series.

Lines 685-690: I am not sure I agree with the authors on the method used: estimating nutrient consumption from nutrient profiles is valid under the assumption that there is no significant impact of lateral transport. If there is horizontal exchange (or mixing), especially in an area with strong horizontal gradients such as in this study, nutrient consumption estimates are highly uncertain. Using the  $T_{min}$  as a criterion, helps to at least constrain the temporal scale of the estimate (i.e. from previous winter), while using other criteria does not. Hence robustness of the estimates given here can hardly be assessed and I doubt values for the different groups can be compared.

#### AUTHOR RESPONSE

Because all nutrient profiles do show surface depletions, they clearly contain information on export (from either local and recent export, or remote and prior export). Extracting the desired local and recent contribution information is difficult for just the reasons the reviewer mentions, and this is why we have pursued two criteria: the traditional temperature minimum based estimate of winter values, and a salinity threshold method designed to evaluate the possibility that this  $T_{min}$  approach overestimates export when the surface depletion is associated with the overlaying of warm salty waters above the  $T_{min}$  layer (via horizontal mixing). We have taken care to emphasize that this makes the depletion estimates uncertain, and to explain how this affects our conclusions, including adding new text:

#### MODIFIED TEXT

This analysis underlines the importance of appropriate winter nitrate (and silicic acid) surface nitrate concentration estimates to the assignment of export magnitudes. We believe the  $S_{threshold}$  approach is the most appropriate given the observed salinity stratification, especially for the relatively weak subsurface thermal stratification observed in the Group 5 stations near the Polar Front.

Given the robustness of the different estimates and the variability (which might be related to both temporal and spatial patterns) I could also argue that there are no significant differences in organic matter (based on N) export between systems. When looking at figure 8 roughly half of the N uptake is lost (either through grazing or sinking). This is consistent with the fact that growth estimates are in the order of roughly one doubling every 3 days while biomass accumulation (from satellite Chla) indicates a doubling very week (between 28/10 and 6/11).

#### AUTHOR RESPONSE

We thank the reviewer for this insightful comment, and we have incorporated it in the revised text, in Results Section 3.5:

#### MODIFIED TEXT

Firstly, given the uncertainties regarding the estimation of nutrient depletions from the profiles, it could be argued that the most robust conclusion is that all the Groups exhibit similar depletions, with roughly half of the N uptake exported and half remaining as accumulated biomass. This is consistent with the growth estimates of roughly one doubling every 3 days and the satellite biomass observations indicating slower doubling approximately each week.

#### AUTHOR RESPONSE

Importantly, we also note that the Abstract emphasizes only this most robust conclusion, that all regions exported similarly:

## MODIFIED TEXT

Comparison of these communities to surface water nitrate (and silicate) depletions as a proxy for export shows that the low biomass recirculation feature had exported similar amounts of nitrogen to the high biomass blooms over the plateau and north of the Polar Front.

Interactive comment on Biogeosciences Discuss., 11, 13841, 2014.

## AUTHOR RESPONSE

### REFERENCES CITED IN OUR RESPONSE TO REVIEWER2

Sweeney, C., Hansell, D. A., Carlson, C. A., Codispoti, L., Gordon, L. I., Marra, J., Millero, F. J., Smith, W. O., and Takahashi, T.: Biogeochemical regimes, net community production and carbon export in the Ross Sea, Antarctica, *Deep Sea Research Part II: Topical Studies in Oceanography*, 47, 3369-3394, 2000.

Uitz, J., Claustre, H., Griffiths, B., Ras, J., and Sandroni, V.: A phytoplankton class-specific primary production model applied to the Kerguelen Islands region (Southern Ocean), *Deep Sea Research I*, 56, 541-560, 2009.

Lasbleiz, M., Leblanc, K., Blain, S., Ras, J., Cornet-Barthaux, V., Hélias Nunige, S., and Quéguiner, B.: Pigments, elemental composition (C, N, P, Si) and stoichiometry of particulate matter, in the naturally iron fertilized region of Kerguelen in the Southern Ocean, *Biogeosciences Discuss.*, 11, 8259-8324, 10.5194/bgd-11-8259-2014, 2014.

Wang, X., Matear, R. J., and Trull, T. W.: Nutrient utilization ratios in the Polar Frontal Zone in the Australian sector of the Southern Ocean: a model, *Global Biogeochemical Cycles*, 17, 1009, doi:10.1029/2002GB001938, 2003.

Laurenceau, E. C., Trull, T. W., Davies, D. M., Bray, S. G., Doran, J., Planchon, F., Carlotti, F., Jouandet, M. P., Cavagna, A. J., Waite, A. M., and Blain, S.: The relative importance of phytoplankton aggregates and zooplankton fecal pellets to carbon export: insights from free-drifting sediment trap deployments in naturally iron-fertilised waters near the Kerguelen plateau, *Biogeosciences Discuss.*, 11, 13623-13673, 10.5194/bgd-11-13623-2014, 2014.

Blain, S., Quéguiner, B., Armand, L., Belviso, S., Bombled, B., Bopp, L., Bowie, A., Brunet, C., Brussaard, C., Carlotti, F., Christaki, U., Corbière, A., Durand, I., Ebersbach, F., Fuda, J. L., Garcia, N., Gerringa, L., Griffiths, B., Guigue, C., Guillem, C., Jacquet, S., Jeandel, C., Laan, P., Lefèvre, D., Lomonaco, C., Malits, A., Mosseri, J., Obernosterer, I., Park, Y.-H., Picheral, M., Pondaven, P., Remenyi, T., Sandroni, V., Sarthou, G., Savoye, N., Scouarnec, L., Souhaut, M., Thuille, D., Timmermans, K., Trull, T., Uitz, J., van-Beek, P., Veldhuis, M., Vincent, D., Viollier, E., Vong, L., and Wagener, T.: Impacts of natural iron fertilisation on the Southern Ocean, *Nature*, 446, 1070-1074, doi:10.1038/nature05700, 2007.

Ebersbach, F., and Trull, T. W.: Sinking particle properties from polyacrylamide gels during the Kerguelen Ocean and Plateau compared Study (KEOPS): Zooplankton control of carbon export in an area of persistent natural iron inputs in the Southern Ocean, *Limnology and Oceanography*, 53, 212-224, 10.4319/llo.2008.53.1.0212, 2008.

Jouandet, M. P., Blain, S., Metzl, N., Brunet, C., Trull, T. W., and Obernosterer, I.: A seasonal carbon budget for a naturally iron-fertilized bloom over the Kerguelen Plateau in the Southern Ocean, *Deep-Sea Research Part II-Topical Studies in Oceanography*, 55, 856-867, 10.1016/j.dsr2.2007.12.037, 2008.

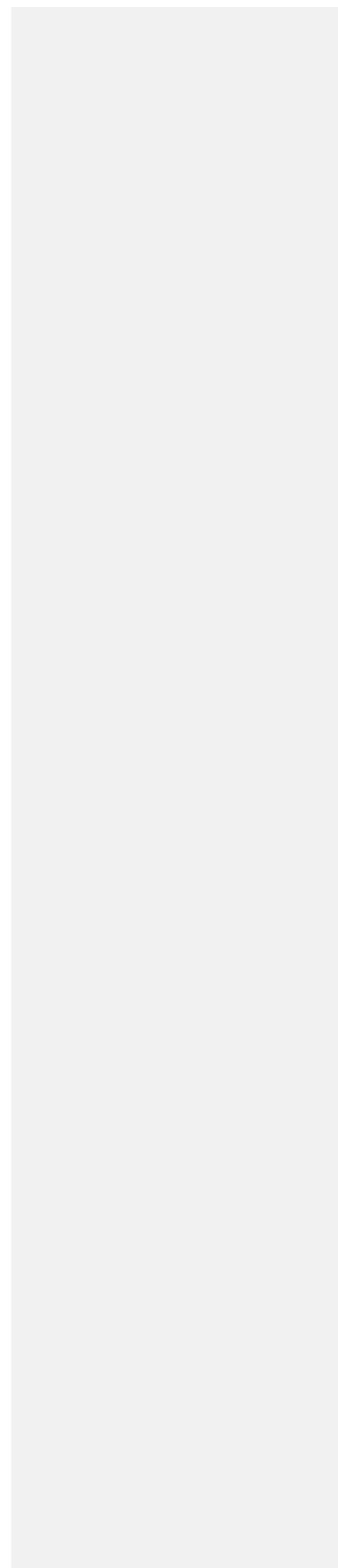
Lampitt, R. S., and Antia, A. N.: Particle flux in deep seas: regional characteristics and temporal variability, *Deep-Sea Research I*, 44, 1377-1403, 1997.

Lutz, M. J., Caldeira, K., Dunbar, R. B., and Behrenfeld, M. J.: Seasonal rhythms of net primary production and particulate organic carbon flux to depth describe the efficiency of biological pump global ocean, *Journal of Geophysical Research*, 112, C10011, doi:10.1029/12006JC003706, 2007.

Keller, K., and Morel, F. M. M.: A model of carbon isotopic fractionation and active carbon uptake in phytoplankton, *Marine Ecology-Progress Series*, 182, 295-298, 1999.

Popp, B. N., Laws, E. A., Bidigare, R. R., Dore, J. E., Hanson, K. L., and Wakeham, S. G.: Effect of phytoplankton cell geometry on carbon isotopic fractionation, *Geochimica et Cosmochimica Acta*, 62, 69-77, 1998.

C6437



1 **Chemometric perspectives on plankton community responses to natural**  
2 **iron fertilization over and downstream of the Kerguelen plateau in the**  
3 **Southern Ocean**

4 T. W. Trull<sup>1, 2, 3\*</sup>, D. M. Davies<sup>1, 2</sup>, F. Dehairs<sup>4</sup>, A.-J. Cavagna<sup>4</sup>, M. Lasbleiz<sup>5</sup>, E. C.  
5 ~~Laurenceau~~~~Laurenceau-Cornec~~~~Cornee~~<sup>1, 2, 3</sup>, F. d'Ovidio<sup>6</sup>, F. Planchon<sup>7</sup>, K. Leblanc<sup>5</sup>, B.  
6 Quéguiner<sup>5</sup> and S. Blain<sup>8, 9</sup>

7

- 8 1. CSIRO Marine and Atmospheric Research, Hobart, Tasmania, Australia  
9 2. Antarctic Climate and Ecosystems Cooperative Research Centre, Hobart, Tasmania, Australia  
10 3. Institute for Marine and Antarctic Studies, University of Tasmania, Hobart, Tasmania, Australia  
11 4. Analytical, Environmental and Geo – Chemistry; Earth Sciences Research Group, Vrije Universiteit  
12 Brussel, Belgium  
13 5. Aix-Marseille Université & Université de Toulon, Marseille, France  
14 6. LOCEAN - IPSL, Université Pierre et Marie Curie, Paris, France  
15 7. Laboratoire des Sciences de l'Environnement Marin (LEMAR), Université de Brest, IUEM, France  
16 8. Sorbonne Universités, UPMC Univ Paris 06, UMR7621, Laboratoire d'Océanographie Microbienne,  
17 Observatoire Océanologique, 66650 Banyuls/mer, France  
18 9. CNRS, Laboratoire d'Océanographie Microbienne, Observatoire Océanologique, 66650 Banyuls/mer,  
19 France

20

21 \*Corresponding author: [Tom.Trull@csiro.au](mailto:Tom.Trull@csiro.au)

22

23

24  
25  
26  
27  
28  
29  
30  
31  
32  
33  
34  
35  
36  
37  
38  
39  
40  
41  
42  
43  
44  
45  
46  
47  
48

### Abstract

We examined phytoplankton community responses to natural iron fertilisation at 32 sites over and downstream from the Kerguelen plateau in the Southern Ocean during the austral spring bloom in October-November 2011. Community structure was estimated from chemical and isotopic measurements (particulate organic carbon POC, <sup>13</sup>C-POC, particulate nitrogen PN, <sup>15</sup>N-PN, and biogenic silica BSi) on size-fractionated samples from surface waters (300, 210, 50, 20, 5, and 1 µm fractions). Higher values of <sup>13</sup>C-POC (vs. co-located <sup>13</sup>C values for dissolved inorganic carbon, <sup>13</sup>C-DIC source values) were taken as indicative of faster growth rates, and higher values of <sup>15</sup>N-PN (vs. co-located <sup>15</sup>N-NO<sub>3</sub> source values) as indicative of greater nitrate use (rather than ammonium use, i.e. higher *f* ratios).

Formatted: Superscript

Community responses varied in relation to both regional circulation and the advance of the bloom. Iron fertilised waters over the plateau developed dominance by very large diatoms (50-210 µm) with high BSi/POC ratios, high growth rates, and significant ammonium recycling (lower *f* ratios) as biomass built up. In contrast, downstream Polar Frontal waters with similar or higher iron supply were dominated by smaller diatoms (20-50 µm) and exhibited greater ammonium recycling. Stations in a deep water bathymetrically trapped recirculation south of the Polar Front with lower iron levels showed the large cell dominance observed on the plateau, but much less biomass. Comparison of these communities to surface water nitrate (and silicate) depletions as a proxy for export shows that the low biomass recirculation feature had exported similar amounts of nitrogen to the high biomass blooms over the plateau and north of the Polar Front. This suggests that early spring trophodynamic and export responses differed between regions with persistent low levels vs. punctual high levels of iron fertilisation.



## 50 1 Introduction

51 Natural iron fertilisation from islands, shelves, and plateaus in the Southern ocean  
52 produces local and downstream elevations of phytoplankton biomass, ~10-fold higher than  
53 in surrounding high nutrient low chlorophyll (HNLC) waters, e.g. (de Baar et al., 1995).  
54 In some of these systems, carbon export has been observed to be elevated ~2-3 fold, e.g.  
55 over the Kerguelen Plateau (Blain et al., 2008; Savoye et al., 2008) and to the north of  
56 Crozet Island (Pollard et al., 2007). But these studies produced order of magnitude  
57 variations in estimates of the amount of carbon export per unit iron supply, as have  
58 deliberate iron fertilisation studies (Boyd et al., 2007). These variations appear to reflect  
59 both observational limitations and system complexity, including the possibility of  
60 variations in initial communities prior to fertilisation (as a result of north-south  
61 oceanographic variations or the extent of connection to coastal habitats).

62 | General principles for expected phytoplankton responses [to iron fertilisation](#) have  
63 been elucidated, though they remain to be fully tested. These include increased growth  
64 rates for all size classes and elevated new production, i.e. increased nitrate use (e.g.  
65 (Armstrong, 1999; Maldonado et al., 2001)). A prevailing view of the overall community  
66 response is that it depends on the interaction of these changes with the response of  
67 zooplankton grazers, which are thought to be more able to keep up with small cell growth  
68 and thus to favour accumulation of larger phytoplankton (Assmy et al., 2013; Morel et al.,  
69 1991). This, in turn, may favour export via either direct sinking or aggregation (Smetacek,  
70 1985; Smetacek, 1998). Variations in diatom life cycles and strategies add seasonal  
71 complexity to this picture (Queguiner, 2013), and the translation of increases in new  
72 production into enhancements in export can be relatively weak, for example, as a result of  
73 strong N recycling (Mosseri et al., 2008).

74 The KEOPS2 expedition sought to examine these and other aspects of community  
75 responses to natural iron fertilisation over and downstream of the Kerguelen plateau, in  
76 austral spring, October-November 2011, as detailed in the multiple papers in this volume.  
77 In this paper, we examine a suite of chemical and isotopic indicators of phytoplankton  
78 community structure and function (chemometrics) and relate them to nitrate (and silicate)  
79 depletion in surface waters as a proxy for carbon export. The following paragraphs provide  
80 an overview of the approach and the structure of the paper.

81 ~~We first~~First, we describe the complex regional circulation, and use it to cluster the  
82 stations into 5 groups (coastal, plateau, waters well downstream near the Polar Front, and  
83 waters in a recirculation close to the plateau - separated into ~~an~~a broad early survey and a  
84 later focused, quasi-Lagrangian time series). For these groups we briefly summarize the  
85 relative levels of iron fertilisation from dissolved and particulate standing stocks (Qu  rou    
86 et al., 2014;van der Merwe et al., 2014) and Fe supply estimates (Bowie et al.,  
87 2014;d'Ovidio et al., 2014). We also assess the elapsed time since iron fertilisation and its  
88 persistence, from seasonal perspectives on vertical mixing (Bowie et al., 2014) and  
89 Lagrangian perspectives on water mass trajectories around the Kerguelen plateau  
90 (d'Ovidio et al., 2014). We also consider two other overarching perspectives on ecosystem  
91 responses: the elapsed time since the beginning of phytoplankton accumulation (from an  
92 animation of satellite ocean colour images; Supplementary Materials), and the level of  
93 biomass enrichment at the time of sampling. Our subsequent chemometric analysis is  
94 undertaken at the level of these 5 Groups, against this framework of relative intensities and  
95 timings of Fe fertilisation and biomass accumulation.

96 Next, we describe ~~the~~our chemometric approach. In brief, i.e. we relied on total  
97 particulate organic carbon (POC) as an indication of eutrophy, size distribution as a  
98 indicator of diversitycommunity structure, biogenic silica /particulate organic carbon



99 (BSi/POC) ratios as a measure of diatom dominance,  $^{13}\text{C}$  as a qualitative metric for growth  
100 rates, and  $^{15}\text{N}$  as a metric for ammonium recycling. ~~For our  $^{13}\text{C}$  and  $^{15}\text{N}$  chemometries,~~  
101 ~~which present methods to estimate rates from standing stocks, we provide a comparison to~~  
102 ~~shipboard incubation results for growth rates and  $f$ -ratios (from  $^{13}\text{C}$  and  $^{15}\text{N}$  tracer uptake~~  
103 ~~experiments, Cavagna et al., 2014this volume).~~ To determine nitrate (and silicic acid)  
104 depletion by the biological pump, we explored both temperature and salinity based  
105 approaches to estimate initial winter surface water concentrations, and also evaluated the  
106 fraction of the observed depletion that still ~~remains~~ remained in the water column for  
107 potential future export using particulate nitrogen and biogenic silica stocks from CTD  
108 casts (Blain et al., 2014;Lasbleiz et al., 2014).

109 These chemometric approaches are not as direct as other methods (such as  
110 microscopy for community structure, incubation experiments for growth rates and  $f$ -ratios,  
111 and sediment trap collections for export), but offer some advantages in terms of  
112 quantitative connections to dissolved nutrient budgets and the ability to examine more  
113 sites. To address these shortcomings, we compared our  $^{13}\text{C}$  growth rate and  $^{15}\text{N}$   $f$ -ratio  
114 estimates to shipboard incubation results from  $^{13}\text{C}$  and  $^{15}\text{N}$  tracer uptake experiments,  
115 (Cavagna et al., 2014), and discuss our more extensive results with respect to information  
116 on community composition from pigment and microscopic analyses (Lasbleiz et al., 2014),  
117 and carbon export from  $^{234}\text{Th}$  depletions (Planchon et al., 2014) and sediment trap  
118 collections (Laurenceau et al., 2014). ~~we arrive at an~~In summary, this provides an  
119 overview of the relative importance of Fe inputs and temporal evolution in the control of  
120 community structure and carbon export in springtime, for the phytoplankton bloom that  
121 forms over and downstream of the Kerguelen plateau.

122

## 123 2 Methods

Formatted: Font: Italic

Formatted: Font: Italic

124 **2.1 Site description**

125           The KEOPS2 campaign was carried out in October - November 2011 over and  
126 downstream of the Kerguelen plateau in the Southern Ocean, under conditions of complex  
127 circulation and rapidly changing phytoplankton biomass, as summarized in Fig-s. 1 and 2,  
128 and further showcased in the full annual satellite chlorophyll animation (Supplement).

129           The Kerguelen plateau is a northwest-southeast oriented seafloor feature which  
130 rises to ~500m below the surface over much of its extent. It also hosts several volcanic  
131 islands, in particular the large Kerguelen Island archipelago in the north and the smaller  
132 Heard Island at the southern edge of the central Kerguelen plateau. The plateau blocks the  
133 eastward flowing Antarctic Circumpolar Current (ACC). Much of the ACC flow goes to  
134 the south of the plateau and through the Fawn Trough (to the south of Heard Island), with  
135 a smaller portion associated with the Subantarctic Front flowing around the northern edge  
136 of Kerguelen island. A narrow jet of ACC water also flows across the plateau in the  
137 narrow, mid-depth (~1000m) channel just to the south of Kerguelen Island (Fig. 1). This  
138 feature corresponds with the northernmost presence of a subsurface temperature minimum  
139 formed by winter cooling (near 200m depth), and thus defines the northernmost branch of  
140 the Polar Front (Park et al., 2014a; Park et al., 2008). This jet was a particularly important  
141 feature of the area sampled during KEOPS2, because it separated the central plateau and  
142 downstream offshore stations to the south of the Polar Front (PF), from those to the north  
143 of the PF, where the coastal stations were also located. As discussed in section 2.2, the  
144 modes of supply of Fe to the waters north and south of this jet may also differ, with some  
145 downstream Polar Front stations potentially influenced by Fe inputs from coastal waters  
146 associated with Kerguelen Island or its shallow northern shelf (d'Ovidio et al., 2014).

147           From a dynamical perspective, the full ocean depth branch of the Polar Front lies  
148 to the south of Heard Island, where the ACC flow transits the Fawn Trough (Sokolov and

149 Rintoul, 2009). As this flow passes to the east of the plateau it follows the bathymetric  
150 contours to the north where it enters a bathymetrically-trapped recirculation region to the  
151 south of the Polar Front, before eventually exiting downstream (d'Ovidio et al., 2014; Park  
152 et al., 2014a). This recirculation feature and the flow along the PF jet are fixed in space by  
153 the bathymetry close to the plateau, but at their eastern edge over the abyssal plain (where  
154 the strong ACC flows passing south and north of the plateau re-join) meandering is strong  
155 and varies with time. For example, the animation of ocean colour (Supplement) suggests  
156 the PF moved southward in this region over the course of the KEOPS2 observations.

157 As shown in Fig. 1, the initial sampling was carried out along a deep water transect  
158 (stations TNS 1-10) run northwards from the central plateau (TNS-10) across the  
159 recirculation feature and Polar Front and into Subantarctic waters (TNS-1). This was  
160 followed by a west to east transect (stations TEW 1-8) running offshore from the  
161 Kerguelen Island coast, across the middle of the recirculation, and reaching the southward  
162 meandering Polar Front in the far east of the study region. This initial survey was followed  
163 by multiple “time-series” visits to the recirculation feature, (designated as stations E1- E5,  
164 with two stations at the E4 time step - to the western side, E4-W, and eastern side, E4-E,  
165 of this recirculation). In addition several other features at the margins of the survey region  
166 were also sampled, with rather complicated nomenclature based on locations, links to  
167 other programs, durations, and purposes:

- 168 – [reference-Reference](#) HNLC waters to the west of the plateau (stations R and R2)
- 169 – A central plateau station that had served as the bloom reference site in the previous  
170 KEOPS campaign in late summer/autumn 2005 (station A3, [sampled twice as A3-  
171 1 and A3-2](#)).

- 172 – High biomass waters in the extreme northeast of the study region, near the  
173 downstream location of the Polar Front (Stations F-L and F-S; L for long, S for  
174 short)
- 175 – Two stations carried out to compare geochemical tracer concentrations in waters  
176 over the plateau (G1) with Kerguelen coastal waters (G2).

177 All of these stations (except TNS-4 and TNS-7) on the initial survey transect were  
178 sampled for our size-fractionated chemometric analyses (with some stations also sampled  
179 both at night and day).

180 The five colour-coded Groups mapped in Fig. 1 cluster the KEOPS2 stations based  
181 largely on the interactions of the circulation with the bathymetry (with some additional  
182 regard for temporal evolution and the timing and extent of iron supply and biomass  
183 accumulation, as discussed below). The properties of these Groups are summarized in  
184 Table 1. In brief, Groups 1 and 2 cluster stations from the recirculation feature. Group 1  
185 consists of stations in this region occupied during the initial transects when biomass was  
186 low, and also ~~for convenience~~ includes the upstream HNLC reference site R2 ([which was](#)  
187 [also sampled early in the voyage](#)). Group 2 holds the stations [subsequently](#) occupied as a  
188 pseudo-Lagrangian time series within the recirculation. Group 3 holds the central plateau  
189 stations, including waters that flow northward to leave the plateau along the south side of  
190 the Polar Front jet. Group 4 [has holds](#) the coastal stations; ~~although the inclusion,~~  
191 [including of TEW-3 is debateable given its location](#) at the plateau edge ([which displayed a](#)  
192 [mix of coastal, plateau, and recirculation properties](#)). Group 5 has the downstream stations  
193 near and north of the Polar Front. Two stations in this Group, at the northern Subantarctic  
194 end of the initial survey, TNS-1 and TNS-2, were included to keep the number of Groups  
195 low, but stand out as quite distinct in having lower biomass with greater proportions of  
196 non-diatom taxa (Lasbleiz et al., 2014), [and are marked by distinct colouring in the figures](#).

197 Additional discussion of stations near the boundaries of these Groups is provided below,  
198 and other clusterings are possible, especially for stations at the boundaries among the  
199 Groups (for further discussion see Lasbleiz et al., 2014). The majority of the analysis  
200 presented in this paper is based on comparisons across these Groups rather than individual  
201 stations (although variations within the Groups do occur and sometimes provide additional  
202 insights, and for this reason the figures display the individual stations in each group in  
203 chronological order (e.g. see Fig. 3).

204

## 205 **2.2 Intensity and timing of Fe fertilisation**

206 Iron sampling and analysis was carried out at a much-reduced subset of the stations  
207 discussed here, albeit with greater vertical resolution (Bowie et al., 2014; Qu  rou   et al.,  
208 2014; van der Merwe et al., 2014). Thus, comparisons to our results are only possible at the  
209 level of our station Groups, and only in a relative sense. The lowest Fe levels were  
210 observed at the HNLC reference station upstream to the west of the Kerguelen Plateau  
211 (slightly less than 0.1 nM at station R2). The recirculation region (Groups 1 and 2) had  
212 low to moderate dissolved Fe (0.06-0.38 nM at stations E2, E3 and E5). Slightly higher  
213 minimum concentrations were observed over the plateau (0.18- 0.21 nM at the Group 3  
214 stations A3-1 and G1). Moderate enrichments were also observed in the Group 5  
215 downstream waters near the Polar Front (~0.26 nM at station F-L). The highest dissolved  
216 Fe levels were in the Group 4 Kerguelen Island coastal waters (surface concentrations of  
217 2.17 nM for TEW 1 and 1.26 nM for TEW 2).

218 Particulate Fe levels were not measured in coastal waters, but generally exceeded  
219 dissolved Fe levels in the Group 3 stations over the plateau (by factors of 13 - 20) and  
220 offshore in the Group 1 and 2 stations in the recirculation feature and the single Group 5  
221 station in the downstream plume (by factors of 2 - 34). The bio-availability of this

222 particulate Fe is unknown, but assuming a conservative fraction of 1% (for discussion see  
223 van der Merwe et al., 2014) leads to a 20% increase over the plateau of available iron and  
224 4-34 % increase offshore.

225 Estimating Fe supply is more difficult. It appears possible that downstream waters  
226 north of the Polar Front (Group 5 stations F-S, F-L, TEW-7, and TEW-8, but not the  
227 Subantarctic influenced stations TNS-1 and TNS-2 ) receives more iron than the plateau  
228 (Group 3) especially in summer when stratification reduces vertical supply over the  
229 plateau, but advection continues to sweep iron-rich coastal waters from the northern  
230 Kerguelen shelf along the northern side of the Polar Front jet (Bowie et al., 2014;d'Ovidio  
231 et al., 2014;Park et al., 2014a).

232 The nature of Fe fertilisation also varies among the regions, in terms of both its  
233 timing relative to our sampling, and its persistence. Recent and brief iron fertilisation  
234 appears likely to characterize the Polar Front (Group 3 region). Water parcel trajectories  
235 calculated from drifter trajectories and altimetry based geostrophic currents (d'Ovidio et al.,  
236 2014) suggest times of less than 0.5 to 1 month for the downstream Polar Front stations  
237 (Group 5 stations F-S, F-L, TEW-7, TEW-8), with rapid dispersal and thus low persistence.  
238 In comparison, it appears to take longer for northern Kerguelen shelf waters to reach the  
239 recirculation region (Group 1 and 2 stations), where the water is then retained for a  
240 relatively long time (30 to 60 days), but is also diluted by approximately equal volumes of  
241 waters derived from the south (d'Ovidio et al., 2014;Park et al., 2014a). These supply  
242 paths are also indicated by Ra isotope distributions (Sanial et al., 2014). Thus fertilisation  
243 of the recirculation feature appears to be less recent and intense than that of the Polar  
244 Frontal region, but probably more persistent. For the Kerguelen coastal stations (Group 4),  
245 where water columns were well mixed to the bottom, fertilisation is both recent and  
246 persistent. Fertilisation over the plateau is also relatively recent in a seasonal context,

247 | ~~having presumably reached a maximum at the time of deepest winter mixing (i.e ~ 2~~  
248 | months from maximum ~~cooling-winter mixing~~ in August-September to sampling in Oct-  
249 | Nov. Its persistence may be similar or somewhat larger than that of the recirculation  
250 | region given estimates of water parcel residence times over the plateau of order 2-3  
251 | months (Park et al., 2008).

252 | In summary, this evaluation of iron inputs yields rank orders as follows:

253 | Intensity of Fe fertilisation (lowest to highest):

254 | *recirculation feature < plateau <≈ Polar Front plume << coastal stations*

255 | Elapsed time since Fe fertilisation and its persistence (most recent to oldest):

256 | *Polar Front plume < recirculation feature <≈ plateau < coastal stations*

257 | For easy reference these properties are summarized for the station Groups in Table 1.

258 |

### 259 | **2.3 Intensity and timing of phytoplankton biomass accumulation**

260 | The KEOPS2 sampling was carried out in spring, spanning the period when  
261 | phytoplankton biomass was rapidly increasing both over and downstream of the plateau,  
262 | forming rather complex patterns in satellite chlorophyll images (Fig. 2). Thus the time of  
263 | sampling relative to the development of surface biomass enrichment varied strongly  
264 | among the stations. The sequence of ocean colour images in Fig. 2. (see also the  
265 | Supplement) suggests that this [chlorophyll increase](#) occurred first in coastal Kerguelen  
266 | island waters (starting in mid-September very close to the island and extending northwards  
267 | by mid October; but reaching only moderate Chl-a levels near  $1 \mu\text{g L}^{-1}$ ), followed by the  
268 | downstream plume north of the Polar Front (near Group 5 stations F-S, F-L, TEW-7,  
269 | TEW-8) where chlorophyll biomass jumped very rapidly from below  $0.5$  to above  $2 \mu\text{g L}^{-1}$   
270 | early in the first week of November.

271 At this time (as shown in the animation in the Supplement), the central plateau and  
272 the recirculation feature still had only minor biomass development, with concentrations  
273 near  $0.5 \mu\text{g L}^{-1}$ . But, within a few days, by 9 November, all strongly Fe enriched regions  
274 (coastal, central plateau, and the downstream waters near the Polar Front) had Chl-a levels  
275 above  $2.5 \mu\text{g L}^{-1}$ . Yet, the recirculation region still had low levels of  $\sim 0.5 \mu\text{g L}^{-1}$  for  
276 another week, and only reached levels of  $1\text{-}1.5 \mu\text{g L}^{-1}$  by end November. Only in early  
277 December, after the end of field sampling, did the recirculation feature reach levels of  $2.5\text{-}$   
278  $3 \mu\text{g L}^{-1}$ . Interestingly, the downstream waters near the Polar Front maintained high levels  
279 throughout most of this period, but the central plateau bloom faded (as sampled by station  
280 A3-2) before being replaced by a second bloom somewhat further east, though still over  
281 the plateau. The animation of these satellite chlorophyll images provides further detail of  
282 the structure and sequence of biomass accumulation, both during and after the voyage  
283 (Supplement).

284 In summary, satellite biomass accumulation yields rank orders as follows:

285 Magnitude of biomass accumulation (lowest to highest, at end of voyage):

286 *recirculation feature < coastal stations < plateau  $\approx$  Polar Front plume*

287 Elapsed time since initiation of biomass accumulation (most recent to oldest):

288 *recirculation feature < Polar Front plume  $\approx$  plateau  $\ll$  coastal stations*

289 For easy reference these properties are summarized for the station Groups in Table 1.

290

## 291 **2.4 Samples**

292

293 This study is based primarily on chemical and isotopic compositions of dissolved  
294 nutrients and size-fractionated particles sampled from surface waters using the ship's clean  
295 seawater supply. Full details of the sample collection and analytical methods are provided  
296 in Appendix A. In brief, particles were analysed for 6 size fractions collected by large



297 volume sequential filtration through a pre-screen (1000µm) and 6 filters (300, 210, 50, 20,  
298 5 and 1 µm pore sizes). These samples were analysed for POC, PN, BSi, <sup>13</sup>C-POC and  
299 <sup>15</sup>N-PN (although BSi could not be analysed on the 1µm fraction, as it was collected with  
300 a quartz filter). Seawater samples collected from the same supply, and also from Niskin  
301 bottles on the CTD system, were analysed for nitrate and dissolved inorganic carbon  
302 concentrations and isotopic compositions (DIC, <sup>13</sup>C-DIC, NO<sub>3</sub><sup>-</sup>, <sup>15</sup>N-NO<sub>3</sub><sup>-</sup>, and <sup>18</sup>O-NO<sub>3</sub><sup>-</sup>).  
303 In addition, [approximately small volume one litre](#) -samples (~~E11~~) were filtered for bulk  
304 POC and PN concentrations and these are reported along with ~~a the~~ total POC ~~that is~~  
305 ~~the~~[determined from the](#) sum of the size fractions. Surface water nitrate concentrations  
306 were continuously mapped using an ultra-violet nitrate sensor.

307 Speaking broadly for all stations, the largest size fractions (300-1000 µm) for the  
308 suspended particles were dominated by zooplankton, primarily copepods. Intact faecal  
309 pellets and phytoplankton aggregates did not contribute significantly to these fractions  
310 (presumably they were disaggregated by the pumping system, because both particle types  
311 were observed in sediment traps equipped with polyacrylamide gels (Laurenceau et al.,  
312 2014); although the presence of intact needles of *Thalassiothrix antarctica* and chains of  
313 *Fragilariopsis kerguelensis* diatoms suggests individual cells were largely undamaged).  
314 The smaller size-fractions were dominated by diatom frustules, with small centric diatoms  
315 abundant on the 5 µm filter, a mix of centric and pennate diatoms on the 20 and 50 µm  
316 filters, and large diatoms and chains of pennate diatoms and small copepods on the 210  
317 µm filter. The particles on the 1 µm quartz filter were too small to examine in any detail  
318 using stereo microscopy. The light beige colour of these filters, in comparison to the  
319 greener shades of the intermediate sizes suggests important contributions from detritus  
320 and/or bacteria ([and absorption of dissolved organic matter onto the 1 µm quartz filters](#)  
321 [may have also occurred, but was not assessed](#)). [These microscopic assessments of the](#)

322 [materials present on the filters are rather limited, and may well have missed significant](#)  
323 [contributions from autotrophs and heterotrophs without frustules or carapaces. Absorption](#)  
324 [of dissolved organic matter onto these filters may have also occurred, but was not](#)  
325 [quantified.](#)

326 [More detailed information on the organisms present on our filters is not available,](#)  
327 but other studies during KEOPS2 of bacterial abundances (Christaki et al., 2014),  
328 phytoplankton (Georges et al., 2014;Lasbleiz et al., 2014), diatom species (L. Armand,  
329 personal communication), and zooplankton (Carlotti et al., 2014) are consistent with our  
330 chemometric interpretation that detritus, bacteria, and phytoplankton contributed to the 1  
331  $\mu\text{m}$  fraction; phytoplankton [and especially diatoms](#) dominated the 5, 20, and 50  $\mu\text{m}$   
332 fractions; a mix of large diatoms and copepods were present in the 210  $\mu\text{m}$  fraction and  
333 copepods, isopods, and occasionally krill were the primary contributions to the 300  $\mu\text{m}$   
334 fraction.

335

## 336 **2.5 Chemometric methods for community structure and function**

337 Evaluation of community structure and function is ideally done via detailed taxonomy  
338 and physiology, but the plethora of organisms makes this very difficult. Chemical  
339 methods offer an easier path with the added advantages of quantitative connections to  
340 dissolved chemical concentrations and budgets. Size fractionation adds value to this  
341 approach, firstly because it provides some separation of phytoplankton (which dominated  
342 the 1, 5, 20, and 50  $\mu\text{m}$  fractions) from heterotrophs (210 and 300  $\mu\text{m}$  fractions), and  
343 secondly because differing sizes of phytoplankton often occupy different biogeochemical  
344 niches (e.g. greater reliance on ammonium by small phytoplankton; -less contribution to  
345 direct export owing to smaller sinking rates) and experience differing ecological couplings

346 (e.g. tighter coupling to grazing control in smaller sizes, because smaller zooplankton have  
347 shorter life cycles).

348         Thus our primary chemometric tool is to simply examine variations in the  
349 distribution of POC across the size fractions as an indicator of community structure. (To  
350 remove the influence of our particular choice of filter sizes, we express the POC  
351 concentration variations as spectra, i.e. we divide the concentrations by the width of each  
352 filtration interval, yielding units of  $\mu\text{M } \mu\text{m}^{-1}$ ). Secondly we use high BSi/POC ratios as  
353 an indication of community dominance by diatoms. ~~(To of course this is simplistic given the~~  
354 presence of silicoflagellates at some stations (Lasbleiz et al., 2014) and the occurrence of a  
355 wide range of BSi/POC ratios in diatoms ~~(Ragueneau et al., 2006), (Ragueneau et al.,~~  
356 ~~2006).~~ ~~and~~ We use low POC /PN ratios as an indication of contributions from  
357 heterotrophic biomass (below the values of ~6-7 that characterise most phytoplankton; ~~e.g.~~  
358 (Anderson and Sarmiento, 1994; Redfield et al., 1963).

359

### 360 **2.5.1 Isotopic chemometric principles – $^{13}\text{C}$**

361         The isotopic chemometric tools are not as common and require greater explanation.  
362 Variations in  $^{13}\text{C}$ -POC and  $^{15}\text{N}$ -PN values derive from both primary photosynthetic  
363 production and the overlay of secondary heterotrophic imprints, especially in the smallest  
364 size fraction (1-5  $\mu\text{m}$ ) in which bacterial processing was important, and the two largest  
365 size fractions (210-300 and 300-1000  $\mu\text{m}$ ) which contained significant contributions from  
366 zooplankton. For the middle size fractions (5-20, 20-50 and 50-210  $\mu\text{m}$ ), biomass was  
367 dominated by phytoplankton and thus these fractions can be used to examine the impacts  
368 of iron fertilisation and other controls on primary production. This is our focus for the use  
369 of these tools. In particular we interpret  $^{13}\text{C}$  enrichment as potentially indicative of higher  
370 growth rates and  $^{15}\text{N}$  enrichment as indicative of higher *f*-ratios (i.e. greater use of nitrate

Formatted: Indent: First line: 1.27 cm

Formatted: Font: Italic

371 in comparison to reduced forms of nitrogen). In the following paragraphs we introduce  
372 quantitative expressions for these relationships, but also acknowledge that they rest on  
373 many assumptions, which we evaluate further in light of our results and are thus indicative  
374 rather than definitive. After this discussion of these autotrophic expressions, we also  
375 briefly describe the scale of heterotrophic effects.

376 Controls on the  $^{13}\text{C}$  composition of phytoplankton are complex, and have been  
377 explored in hundreds of papers since an early survey of the variability in marine carbon  
378 isotopic compositions (Craig, 1953), with occasional significant advances and reviews,  
379 e.g. (Farquhar et al., 1982; Goericke et al., 1994; Laws et al., 1995; Laws et al., 2002; Rau et  
380 al., 1996; Schulz et al., 2007; Tortell et al., 2008). In brief, there are two main causes for  
381  $^{13}\text{C}$  variations of any given phytoplankton cell. Firstly, the cell  $^{13}\text{C}$  content depends on the  
382 chemical form of DIC that is assimilated, because the less abundant aqueous molecular  
383  $\text{CO}_2$  form contains much less  $^{13}\text{C}$  than the bicarbonate anion form which makes up more  
384 than 90% of the total DIC. At the temperatures pertaining during the KEOPS study, this  
385 equilibrium fractionation lowers the  $^{13}\text{C}$  content of aqueous molecular  $\text{CO}_2$  by ~11‰ (Rau  
386 et al., 1997):

$$387 \quad \frac{^{13}\text{C-CO}_2}{^{13}\text{C-DIC}} = \frac{+23.644 - 9701.5/T_{\text{kelvin}}}{1000} \quad (1)$$

388 Secondly, the cell  $^{13}\text{C}$ -POC content depends on the extent to which the enzymatic kinetic  
389 discrimination against  $^{13}\text{C}$  during photosynthetic carbon fixation (of 20-30 ‰, varying  
390 with the specific metabolic pathways) is expressed. It is only fully expressed when  
391 inorganic carbon flow into and out of the cell (supply) is faster than fixation (demand).  
392 Both these effects often lead to higher  $^{13}\text{C}$  contents in faster growing cells, because faster  
393 growth favours use of the more abundant bicarbonate form of DIC and also leads to less  
394 expression of the kinetic fractionation.

Formatted: Not Highlight

395 Thus the association of higher  $^{13}\text{C}$  contents with faster growing cells is very strongly  
396 justified for any particular phytoplankton species, from both metabolic understanding and  
397 the plethora of batch and chemostat experimental studies. Despite this understanding,  
398 inferring growth rates for communities of phytoplankton from field measurements of  $^{13}\text{C}$ -  
399 POC is fraught with difficulties. The magnitudes of these two main isotopic effects vary  
400 strongly among different phytoplankton (and with their conditions of growth including  
401 temperature, nutrient and trace metal availability, light levels, specific enzymatic pathways,  
402 etc. (Burkhardt et al., 1999b; Burkhardt et al., 1999c; Fontugne et al., 1991; Schulz et al.,  
403 2007)), and there is no universal quantitative relationship between growth rate and  
404 phytoplankton  $^{13}\text{C}$  content. In particular, cell size is a key variable in the control of  $^{13}\text{C}$   
405 contents (Popp et al., 1999; Rau et al., 1996; Rau et al., 1997; Rau et al., 1990). This effect  
406 is so important that the global range of surface water bulk  $^{13}\text{C}$ -POC values can be  
407 observed across different size fractions within a single Southern Ocean sample (Trull and  
408 Armand, 2001). Good correlations between growth rates and  $^{13}\text{C}$  contents when cell size  
409 is expressed in terms of the surface/volume ratio suggest this results from the balance of  
410 supply versus demand (Popp et al., 1998b), of either or both aqueous  $\text{CO}_2$  and bicarbonate  
411 forms (Burkhardt et al., 1999a; Keller and Morel, 1999; Schulz et al., 2007), and with  
412 further modulation by other environmental controls such as the availability of light and  
413 other nutrients (Burkhardt et al., 1999c; Gervais and Riebesell, 2001; Schulz et al., 2004).  
414 This complexity means that our observed  $^{13}\text{C}$ -POC variations, even within a given size  
415 fraction, could arise by multiple mechanisms. Higher  $^{13}\text{C}$  contents could reflect faster  
416 growth rates (via either greater use of bicarbonate or an increase of fixation of all DIC  
417 chemical forms relative to supply), or might instead reflect changes in species with  
418 inherently different uptake and assimilation metabolisms, or changes in metabolism driven  
419 by other controls such as light or iron availability. Our chemometric methods cannot

420 distinguish among these possible causes, and thus our expression of the  $^{13}\text{C}$ -POC  
 421 variations in terms of growth rate variations can only be viewed as an indicative exercise.  
 422 To pursue this, we chose a model fit to chemostat data (Popp et al., 1998b):  
 423 
$$^{13}\text{C}\text{-POC} = (^{13}\text{C}_{\text{source}} - \epsilon_p) + k \text{ demand-rate/supply-rate} \quad (2)$$
  
 424 in which the first term expresses the lowest possible  $^{13}\text{C}$  contents of the cell as growth rate  
 425 approaches zero, and the second term describes the linear (constant k) dependence of  
 426 isotopic composition on the relative rates of  $\text{CO}_2$  supply into the cell and its cellular  
 427 fixation. Popp et al. (1998) assumed the chemical form was aqueous molecular  $\text{CO}_2$  but  
 428 further evaluation showed that the data could also be fit by a model allowing either or both  
 429  $\text{CO}_2$  and bicarbonate uptake (Keller and Morel, 1999). Both models assume that the  
 430 supply rate depends linearly on its external concentration modulated by the surface area of  
 431 the cell, and thus while the fitting constants we use here are from Popp et al (1998), the  
 432 scaling to the surface/volume ratio (S/V) of the cell is independent of the chemical form of  
 433 uptake):

434 
$$^{13}\text{C}\text{-POC} = (^{13}\text{C}\text{-CO}_2 - 25) + 182 \mu / ([\text{CO}_2] \text{ S/V}) \quad (3)$$

435 Rewriting this equation for growth rate,  $\mu$ , and our measured  $^{13}\text{C}$ -DIC and  $^{13}\text{C}$ -POC values  
 436 yields an indicative path to possible growth rates for our size fractions:

437 
$$\mu = \text{S/V} [\text{CO}_2] [^{13}\text{C}\text{-POC} - (^{13}\text{C}\text{-CO}_2 - 25)] / 182 \quad (4)$$

438 with  $^{13}\text{C}\text{-CO}_2$  calculated using equation (1),  $[\text{CO}_2]$  obtained from underway  $\text{pCO}_2$   
 439 observations (Lo Monaco et al., 2014) and Henry's Law (Weiss, 1974). In this expression,  
 440 growth rate  $\mu$  is in  $\text{d}^{-1}$ , S/V in  $\mu\text{m}^{-1}$ , and  $[\text{CO}_2]$  in  $\mu\text{mol kg}^{-1}$ .

441 This expression provides growth rates that we compare to other estimates. Of course,  
 442 comparison of these rates is very sensitive to S/V estimates, as well as to all the other  
 443 possible sources of variations in  $^{13}\text{C}$  contents summarized above. For example, a 30%  
 444 increase in the mean size of cells, such as could occur within a given size fraction, would

Formatted: Font: Italic

445 yield a 69% increase in the model growth rate (for spherical cells). For this reason, our  
446 growth rate estimates must be viewed with great caution, not only in terms of their  
447 absolute magnitudes, but also in terms of their relative magnitudes across the different  
448 stations.

449 In comparison to these fractionation effects accompanying primary production, trophic  
450 <sup>13</sup>C enrichment is thought to be relatively small within a given class of compounds for  
451 carbon (~ 1‰ per trophic level; (Michener and Schell, 1994)). However, accumulation of  
452 lipids, which are <sup>13</sup>C depleted owing to their multi-step synthesis pathways, causes many  
453 zooplankton to have lower <sup>13</sup>C contents than their diet (Michener and Schell,  
454 1994; Syvaranta and Rautio, 2010). This is a probable contributor to the <sup>13</sup>C-POC values  
455 of the two largest size fractions, as discussed in the results section.

456 Finally, because our focus is on extracting information about growth conditions for the  
457 communities at the time of sampling, we remove the influence of source inorganic carbon  
458 isotopic composition spatial variations on the <sup>13</sup>C-POC variations, by examining their  
459 offset relative to the source:  $^{13}\text{C-POC}_{rs} = ^{13}\text{C-POC} - ^{13}\text{C-DIC}$ .

460 Controls on the <sup>13</sup>C composition of phytoplankton are complex (Goericke et al., 1994),  
461 but in general, within a phytoplankton size class (and relative to source compositions) <sup>13</sup>C  
462 enrichment is a sign of faster growth (Popp et al., 1998b; Popp et al., 1999; Rau et al.,  
463 1997; Trull et al., 2008). In other words, discrimination against <sup>13</sup>C assimilation is less  
464 strong in rapidly growing cells. We briefly review the processes involved in this  
465 discrimination to inform our use of <sup>13</sup>C-POC variations to estimate approximate growth  
466 rates, and return to this issue again in the results section in light of the specifics of the  
467 KEOPS2 observations.

468 One possible control is a change from use of the scarce molecular CO<sub>2</sub> form of DIC to  
469 greater use of the ~100 fold more abundant bicarbonate form (although this form is

470 electrically charged and thus likely to be more energetically costly to assimilate).

471 Assimilation of bicarbonate raises  $^{13}\text{C}$  POC, because it has much higher  $^{13}\text{C}$  contents than  
472 dissolved molecular  $\text{CO}_2$  (~11% higher at KEOPS2 temperatures, as expressed by the  
473 approximate equilibrium fractionation expression (Rau et al., 1997):

$$474 \quad {}^{13}\text{C} \text{ CO}_2 = {}^{13}\text{C} \text{ DIC} + 23.644 - 9701.5/T_{\text{kelvin}} \quad (1)$$

475 There is presently no understanding of how a possible switch from  $\text{CO}_2$  to  $\text{HCO}_3^-$   
476 assimilation might depend on growth rate, but some aspect of the relative availability of  
477  $\text{CO}_2$  supply versus demand is likely to be involved. This balance also affects  
478 the extent of fractionation that occurs if only one external species (e.g. molecular  $\text{CO}_2$ ) is  
479 assimilated, and models of supply versus demand have been shown to reproduce  $^{13}\text{C}$   
480 variations well for many phytoplankton (e.g. Rau et al., 1997; Popp et al., 1998), and we  
481 rely on this approach to re-express our field  $^{13}\text{C}$  variations in terms of (relative) growth  
482 rates.

483 The discrimination against  $^{13}\text{C}$  that accompanies intra-cellular enzymatic fixation of  
484  $\text{CO}_2$  ( $\epsilon_i$  ~25-28‰ for the most common enzymes but less for other forms) exceeds the  
485 isotopic offset between the external DIC species, and thus has been a focus for the likely  
486 control on fractionation during carbon assimilation. The extent to which this enzymatic  
487 discrimination is expressed in the  $^{13}\text{C}$  POC depends on the balance of supply into the cell  
488 versus demand from growth. If all supply is assimilated  $^{13}\text{C}$  POC equals the supply  
489 value, but if little is assimilated (with the rest re-exported), the full enzymatic fractionation  
490 occurs (i.e.  $^{13}\text{C}$  POC approaches the supply value minus  $\epsilon_i$ ). Laboratory experiments have  
491 confirmed the general validity of the supply versus demand model and shown (for a  
492 limited set of phytoplankton) that  $^{13}\text{C}$  POC increases linearly with growth rate (Popp et al.,  
493 1998b). Specifically, Popp et al. (1998) applied the model that:

$$494 \quad {}^{13}\text{C} \text{ POC} = ({}^{13}\text{C}_{\text{source}} - \epsilon_i) + k \text{ demand rate/supply rate} \quad (2)$$



495 in which the first term expresses the lowest possible  $^{13}\text{C}$  contents of the cell as growth rate  
496 approaches zero, and the second term describes the linear (constant k) dependence of  
497 isotopic composition on the relative rates of  $\text{CO}_2$  supply into the cell and its cellular  
498 fixation. They found an excellent fit to data by assuming the chemical form is aqueous  
499 molecular  $\text{CO}_2$  and that supply rate depends linearly on its external concentration  
500 modulated by the surface to volume ratio ( $S/V$ ) of the cell:

Formatted: Font: Italic

$$^{13}\text{C POC} = (^{13}\text{C CO}_2 - 25) + 182 \mu / ([\text{CO}_2] S/V) \quad (3)$$

Formatted: Font: Italic

502 Rewriting this equation for growth rate,  $\mu$ , and our measured  $^{13}\text{C}$  DIC and  $^{13}\text{C}$  POC values  
503 yields a possible path to quantitative growth rates for our size fractions:

$$\mu = S/V [\text{CO}_2] [^{13}\text{C POC} - (^{13}\text{C CO}_2 - 25)] / 182 \quad (4)$$

Formatted: Font: Italic

505 with  $^{13}\text{C CO}_2$  calculated using Eq. equation (1),  $[\text{CO}_2]$  obtained from underway  $\text{pCO}_2$   
506 observations (Lo Monaco et al., this volume 2014) and Henry's Law (Weiss, 1974). In this  
507 expression, growth rate  $\mu$  is in  $\text{d}^{-1}$ ,  $S/V$  in  $\mu\text{m}^{-1}$ , and  $[\text{CO}_2]$  in  $\mu\text{mol kg}^{-1}$ :

Formatted: Font: Italic

508 As discussed further in the results section, this expression predicts two useful things.  
509 Firstly, it predicts growth rates that we compare to other estimates. Secondly it shows that  
510 a given  $^{13}\text{C}$  POC increase predicts a larger increase in growth rate for small cells than for  
511 large cells, because smaller cells have higher  $S/V$  (and this sensitivity to  $S/V$  is  
512 large). Of course, comparison of these rates is sensitive to  $S/V$  estimates and to the  
513 assumption that transport into and out of the cell scales with this parameter. For this  
514 reason, our growth rate estimates must be viewed with great caution.

Formatted: Font: Italic

Formatted: Font: Italic

Formatted: Font: Italic

515 Trophic  $^{13}\text{C}$  enrichment is thought to be relatively small within a given class of  
516 compounds for carbon ( $\sim 1\%$  per trophic level; (Michener and Schell, 1994)). However,  
517 accumulation of lipids, which are  $^{13}\text{C}$  depleted owing to their multi-step synthesis  
518 pathways, causes many zooplankton to have lower  $^{13}\text{C}$  contents than their diet (Michener

519 and Schell, 1994; Syvaranta and Rautio, 2010). ~~This is a probable contributor to the  $^{13}\text{C}$ -~~  
520 ~~POC values of the two largest size fractions, as discussed in the results section.~~

521 ~~Finally, because our focus is on extracting information about growth conditions for the~~  
522 ~~communities at the time of sampling, we remove the influence of source inorganic carbon~~  
523 ~~isotopic composition spatial variations on the  $^{13}\text{C}$  POC variations, by considering only~~  
524 ~~their offset relative to the source  $\epsilon_{\text{rs}}$ :  $^{13}\text{C POC}_{\text{rs}} = ^{13}\text{C POC} - ^{13}\text{C DIC}$ .~~

525

## 526 2.5.2 Isotopic chemometric principles – $^{15}\text{N}$

527 Phytoplankton  $^{15}\text{N}$ -PN variations result primarily from the relative use of reduced  
528 nitrogen (mainly ammonium) which has low  $^{15}\text{N}$  contents vs. the more abundant nitrate  
529 pool which has higher  $^{15}\text{N}$  contents, and secondarily from variations in the isotopic  
530 fractionation accompanying nitrate assimilation (Goericke et al., 1994; Karsh et al.,  
531 2003; 2014; Trull et al., 2008). As with the carbon isotopes, we discuss the  $^{15}\text{N}$ -PN  
532 variations relative to co-located  $^{15}\text{N}$ - $\text{NO}_3$  source values ( $^{15}\text{N-PN}_{\text{rs}} = ^{15}\text{N-PN} - ^{15}\text{N-NO}_3$ ), to  
533 separate source composition effects (that have accumulated from the history of nitrogen  
534 metabolism in a given parcel of water) from the fractionation associated with current PN  
535 production. This source composition effect was larger for nitrogen than for carbon,  
536 because variation in  $^{15}\text{N-NO}_3$  values was larger (6.1 to 8.0‰), and  $^{15}\text{N-PN}$  variations were  
537 smaller (6‰).

538 By estimating expected values for  $^{15}\text{N-PN}_{\text{rs}}$  formation from nitrate and from  
539 ammonium, estimates of new vs. recycled production (i.e.  $f$  ratios) can be obtained for  
540 each size fraction by mass balance. The observed range of fractionation factors for nitrate  
541 assimilation during KEOPS2, namely  $\epsilon_{\text{na}}$  of -4 to -4.5 ‰, as estimated from  $^{15}\text{N-NO}_3$   
542 variations in the water column (Dehairs et al., 2014), provides an upper limit for growth  
543 on nitrate of  $^{15}\text{N-PN}_{\text{rs}}$  (-4‰). For ammonium, the simplest approximation is to use a value

544 just below the lowest observed  $^{15}\text{N-PN}_{\text{rs}}$ , i.e. to assume that these cells grew on  
545 ammonium alone (Trull et al., 2008). Using these end members ( $^{15}\text{N-PN}_{\text{Nrs}} = -4 \text{ ‰}$  for  
546 growth on nitrate;  $^{15}\text{N-PN}_{\text{Ars}} = -8 \text{ ‰}$  for growth on ammonium), yields  $f$  ratio estimates  
547 for each size-fraction, from:

$$548 \quad f = \frac{(^{15}\text{N-PN}_{\text{rs}} - ^{15}\text{N-PN}_{\text{Ars}})}{(^{15}\text{N-PN}_{\text{Nrs}} - ^{15}\text{N-PN}_{\text{Ars}})} \quad (5)$$

549 In comparison to carbon, trophic enrichment of  $^{15}\text{N}$  is relatively large ( $\sim 3 \text{ ‰}$  vs  $\sim 1 \text{ ‰}$ ;  
550 (Michener and Schell, 1994; Wada and Hattori, 1978), which provides a cautionary note on  
551 the interpretation of the  $f$  ratio estimates. The largest zoo-plankton containing size  
552 fractions (210-300  $\mu\text{m}$ , 300-1000  $\mu\text{m}$ ) have higher  $^{15}\text{N-PN}_{\text{rs}}$  values than are achievable by  
553 primary production and derive from this process.

554

### 555 3 Results

#### 556 3.1 Total biomass variations

557 POC biomass concentrations in surface waters varied from  $\sim 3$  to  $25 \mu\text{M}$  (Table 2),  
558 reported as the “total” sum of fractions as filtered from as much as 2600 L of underway  
559 supply water, and are in agreement with our 1 L single filter “bulk” filtrations (Appendix  
560 A). Although there are-were some differences in POC results across the multiple sample  
561 methodologies of the entire mission-KEOPS2 program e.g. from underway supply, Niskin  
562 bottles, and in-situ pumps (Dehairs et al., 2014; Lasbleiz et al., 2014; Tremblay, 2014),  
563 these remain to be fully assessed and hence here we focus on our own internally consistent  
564 results.

565 There were significant variations of POC concentrations within the Groups as well  
566 as among them (Fig. 3). The Group 1 upstream Fe-poor HNLC reference station R2 and  
567 the early sampled furthest south and coldest Group 3 plateau station A3-1 had the lowest  
568 values. The recirculation initial survey stations in Group 1 had somewhat higher values

569 (5-10  $\mu\text{M}$ ; with a single higher value of 15  $\mu\text{M}$  at TEW-4, [attributable to a high](#)  
570 [heterotrophic contribution to its largest size fractions](#)), with little increase over time as  
571 represented by the Group 2 recirculation time series (again with a single outlier at E4-E).  
572 The Group 5 downstream Polar Front bloom stations had the highest biomasses, exceeding  
573 all but 1 of the Group 3 Plateau stations as well as all Group 4 coastal stations. Note that  
574 the Group 5 stations from warmer waters north of and near the Subantarctic front (TNS 1  
575 and 2), where the upstream flow may not cross the Kerguelen shelf, stand out from the  
576 other Group 5 stations as having much lower biomass, similar to the upstream HNLC  
577 reference station (R2). This distribution of POC among the Groups provides important  
578 results: (i) waters that have not crossed the plateau have low biomass, presumably  
579 reflecting a lack of Fe fertilisation, and (ii) downstream blooms achieve higher  
580 concentrations of biomass than coastal blooms. Given that Fe concentrations were highest  
581 in the coastal waters (Table 1; section 2.2), this means that ecosystem dynamics must also  
582 contribute importantly to the control of biomass.

583 Distributions of POC with particle size also varied significantly (Fig. 3). All  
584 stations exhibited the highest concentrations in the smallest size fraction (1-5  $\mu\text{m}$ ) *when*  
585 *normalized to the width of this fraction interval* (Fig. 3), but these concentrations were  
586 relatively constant across the Groups. In contrast the concentrations in the three  
587 phytoplankton dominated intermediate size fractions (5, 20, 50  $\mu\text{m}$  filters) varied among  
588 the groups, and drove the total POC biomass changes described above. There were  
589 significant variations within these 3 size fractions as well. Abundance decreased  
590 monotonically with size at the HNLC reference station. The Group 1, and even more so  
591 the Group 2, stations exhibited greater increases (as total biomass increased either among  
592 stations in Group 1 or with time in the Group 2 time series; note that Table 2 lists all  
593 stations in chronological order) in the 20  $\mu\text{m}$  fraction than the 5  $\mu\text{m}$  fraction, but still low

Formatted: Font: Not Italic

594 values in the 50  $\mu\text{m}$  fraction. The Group 3 plateau stations started with this slightly  
595 “humped” (i.e. ~~5 < 20 > 50  $\mu\text{m}$~~ ) POC distribution (i.e. POC higher in the 20  $\mu\text{m}$  fraction  
596 than in both the 5 and 50  $\mu\text{m}$  fractions), but as biomass increased with time the 50  $\mu\text{m}$   
597 fraction came to dominate. Interestingly, this never occurred in the Group 4 coastal or  
598 Group 5 Polar Frontal biomass rich stations, which remained dominated by the 20  $\mu\text{m}$  size  
599 fraction.

600 Heterotrophic biomass (as represented by the two largest size filters, 210 and 300  
601  $\mu\text{m}$ ) was generally an order of magnitude lower than autotrophic biomass (as represented  
602 by the 3 intermediate fractions), and more than 2 orders of magnitude lower if the smallest  
603 fraction is also included as an autotroph fraction. ~~Heterotrophic biomass~~ generally  
604 increased with total biomass in all the Groups, except the Group 4 coastal waters. As  
605 mentioned earlier, ~~Station-station~~ TEW-4 in Group 1 had unusually high heterotrophic  
606 biomass, which explains its outlier status of exceptionally high total POC for this Group.

607

### 608 **3.2 Variations in BSi concentrations and associated contributions to biomass**

609 BSi estimates were not possible for the smallest size fraction (owing to use of a  
610 quartz 1  $\mu\text{m}$  filter). Thus total BSi is underestimated, and comparisons to total POC must  
611 be done cautiously. As shown in Fig. 3 (top row), the highest BSi levels were observed in  
612 the Plateau stations late in the voyage, with these exceeding those of the Group 5 Polar  
613 Frontal bloom stations as well as all the other Groups. The lowest levels were in the Polar  
614 Frontal Zone and Subantarctic stations (Group5, stations TNS1 and 2). More detailed  
615 evaluation is possible on a size-fractionated basis. The initial survey of Group 1 low  
616 biomass waters found a wide range of BSi/POC ratios that covered most of the variability  
617 seen across the entire KEOPS2 study (Fig. 3; bottom row). Among the other groups, the  
618 Group 3 plateau stations stands out for having high BSi/POC ratios in all the autotrophic

619 fractions (5, 20, 50  $\mu\text{m}$  filters), in contrast to uniformly low ratios for the Group 5 stations.  
620 The presence of non-zero BSi/POC ratios in many of the largest, zooplankton dominated  
621 size fractions (210 and 300  $\mu\text{m}$  filters) reflects the presence of chain-forming diatoms,  
622 although their POC biomass was insignificant in comparison to that of the autotrophic  
623 intermediate fractions.

624 Much of the range in BSi/POC ratios for the intermediate size fractions overlaps  
625 with that expected for diatoms under iron-impoverished (BSi/POC  $\sim 0.6$ ) to iron-replete  
626 (BSi/POC  $\sim 0.15$ ) conditions (Hoffman et al., 2007; Hutchins and Bruland, 1998; Takeda,  
627 1998), but note that this is a simplistic view of diatom BSi/POC variations in response to  
628 Fe inputs which ignores variations across taxa and across life cycle stages (Leynaert et al.,  
629 2004; Marchetti and Cassar, 2009; Ragueneau et al., 2006). There was no clear  
630 correspondence across the groups between BSi/POC values and Fe fertilisation levels, in  
631 that the Group 4 Fe-rich coastal waters had intermediate BSi/POC ratios in comparison to  
632 the moderately Fe-rich Group 3 plateau and Group 5 downstream Polar Front waters.  
633 Community variations in the ratio of diatom to non-diatom taxa thus appear to overprint  
634 any dependence [of diatom BSi/POC ratios](#) on Fe ~~for levels diatom BSi/POC ratios~~.  
635

### 636 **3.3 $^{13}\text{C}$ variations**

637 We first note that the  $^{13}\text{C}$ -POC<sub>TS</sub> values of the HNLC reference station (R-2) were  
638 the lowest of all stations, and we take them as an indication of expectations for slowly  
639 growing offshore polar phytoplankton (Fig. 4). In comparison, Group-1 and Group-2  
640 stations (which had indistinguishable  $^{13}\text{C}$ -POC<sub>TS</sub> values), were elevated by  $\sim 2\%$  (ranging  
641 from 1 to 4‰) in comparison to the R-2 HNLC reference level. These stations also  
642 displayed an increase in  $^{13}\text{C}$ -POC<sub>TS</sub> values from the smallest (1-5  $\mu\text{m}$ ) towards larger size  
643 fractions (5-20, 20-50  $\mu\text{m}$ ) before decreasing again in the largest autotrophic size fraction

644 (50-210  $\mu\text{m}$ ) and generally also in the heterotrophic dominated- size fractions (210-300  
645 and 300-1000  $\mu\text{m}$ ). This hump-shaped pattern was also present at the Group-3 plateau  
646 stations, where  $^{13}\text{C}$ -POC<sub>rs</sub> values were elevated further. The Group-4 coastal stations had  
647 the highest  $^{13}\text{C}$ -POC<sub>rs</sub> values, with values as high as -20‰.

648 This pattern has been found before in Antarctic polar waters, with the initial  
649 increase in  $^{13}\text{C}$ -POC<sub>rs</sub> with size attributed to the effect of decreasing surface/volume on  
650 CO<sub>2</sub> uptake (Popp et al., 1998a;Popp et al., 1999), and the subsequent decrease in larger  
651 fractions attributed to the presence of needle-shaped diatoms with high surface/volume  
652 ( $S/V$ ) ratios similar to small cells (Trull and Armand, 2001). Detailed  $S/V$  estimates for  
653 our samples are not yet available to assess this explanation or the influence of the presence  
654 of chains of *Fragillariopsis kerguelensis*, *Eucampia antarctica*, and *Chaetoceros*  
655 *hyalochaeta* diatoms which contribute strongly to the larger autotrophic size fractions at  
656 many stations (Armand et al., personal communication, 2014). The presence of lipid-rich  
657 zooplankton in the two largest size fractions is another probable cause of their low  $^{13}\text{C}$ -  
658 POC values, [based on low  \$^{13}\text{C}\$ -POC values for zooplankton collected with nets during  
659 KEOPS2](#) (Carlotti et al., 2014), ~~but one that we are unable to explore further.~~

Formatted: Superscript

660 To translate our observed  $^{13}\text{C}$ -POC variations (in the autotrophic size classes) to  
661 growth rates using the relationships described in the Methods (section 2.5.1), we must  
662 make some assumptions about the size and shapes of the phytoplankton in the different  
663 filter fractions. This choice is difficult in the absence of detailed observations, and we  
664 took a very simple approach of representing the phytoplankton as rectangular prisms with  
665 square cross-sections, with the dimensions given in Table 3 for the 1, 5, 20, and 50  $\mu\text{m}$   
666 filter fractions. For the two larger fractions, we assumed diatoms were predominantly  
667 present as chains (based on microscopy; Armand et al., personal communication, 2014),  
668 and that the surface for CO<sub>2</sub> exchange was accordingly reduced (the details accompany

669 Table 3). These assumptions are of course tenuous because diatom chains vary in their  
670 morphology, and of course the relationship between  $S/V$  and uptake is itself a large  
671 assumption, [in that it presupposes that both diffusive and active inorganic carbon uptake](#)  
672 [scale with cell surface area \(see Methods for additional discussion of the uncertainties in](#)  
673 [estimating growth rates from  \$^{13}\text{C}\$ -POC contents\)](#). Nevertheless, on this basis, we obtained  
674  [\$^{13}\text{C}\$  model](#) growth rate variations for each of the autotrophic size fractions (Table 2) and  
675 total community growth rates (Fig. 5) for each station by summing results for the four  
676 smallest size fractions (1, 5, 20, 50  $\mu\text{m}$ ). Similar variations across the stations were  
677 obtained by limiting the sum to the 5, 20, and 50  $\mu\text{m}$  fraction results (data not shown).

678 The  [\$^{13}\text{C}\$  model](#) growth rates decreased with size across the size fractions (from the 1 to the  
679 50  $\mu\text{m}$  filter) by factors of 10 to 15, in excellent agreement with allometric relationships  
680 assembled for a much broader range of phytoplankton, although the high growth rates of 2  
681 to 3  $\text{d}^{-1}$  in the smallest fraction are greater than expected for polar waters (Chisholm,  
682 1992;Cózar and Echevarría, 2005). [This could reflect significant contributions from](#)  
683 [detritus from larger autotrophs and bacteria in this fraction, or other errors in the model](#)  
684 [\(see the Methods section for discussion of the low fidelity of the  \$^{13}\text{C}\$  model growth rates\)](#).

685 Our community (sum of fractions)  [\$^{13}\text{C}\$  model](#) growth rates compare reasonably  
686 well with a limited set of incubation results, calculated by integrating results from  
687 different light level deck onboard incubations (Cavagna et al., 2014) over the depth of the  
688 surface mixed layers as shown in Table 4 (Park et al., 2014b;Park et al., 2014a).

689 The overall dynamic range of the incubation and model growth rates was identical  
690 ( $0.18 \text{ d}^{-1}$ ). For the model this ranged from  $0.08 \text{ d}^{-1}$  at the coldest early-sampled low  
691 biomass station over the plateau (A3-1) to  $0.27 \text{ d}^{-1}$  at coastal station TEW-2. The  
692 incubations ranged from a low value of  $0.065 \text{ d}^{-1}$  at the HNLC reference station (A3-1 was  
693 not studied) to a high of  $0.24 \text{ d}^{-1}$  at the Group 5 Polar Front station F-L (coastal stations

Formatted: Superscript

Formatted: Superscript

Formatted: Superscript

Formatted: Superscript

Formatted: Indent: Left: 0 cm, First line: 1.27 cm



694 were not studied). Overall correlation between the 8 pairs of results from the same stations  
695 (though not sampled at identical times) was very poor ( $r^2 < 0.1$ ) but this was driven by  
696 strong disagreement at the single Group 5 downstream Polar Front station where the  
697 incubations found their highest depth integrated growth rate ( $0.24 \text{ d}^{-1}$  at F-L) but our  $^{13}\text{C}$ -  
698 based estimates were much lower, and without this pair, the correlation was reasonably  
699 strong ( $r^2 = 0.67$ ).

700 |       Given the importance of  $S/V$  variations to the  $^{13}\text{C}$  model growth rate estimates (see  
701 | [the Methods section](#)), variations between Groups with similar size distributions and  
702 | phytoplankton flora (the Group 1, 2 recirculation and Group 3 plateau stations) are  
703 | probably more reliably assessed than variations between Groups with more distinct flora  
704 | (coastal Group 4 stations and downstream Polar Front Group 5 stations). The Group 2  
705 | recirculation time series showed quite constant and moderate growth rates ( $0.17 - 0.19 \text{ d}^{-1}$ ).  
706 | Interestingly, values during the earlier Group 1 initial survey were somewhat higher in this  
707 | region ( $0.19 - 0.21 \text{ d}^{-1}$ ), and reached  $0.23 \text{ d}^{-1}$  at the southern end of the north-south transect  
708 | over the plateau (TNS 9, 10). Later sampled Group 3 plateau stations (A3-2, G1, E4W,  
709 | E4W2) also had high  $^{13}\text{C}$  model growth rates ( $0.19 - 0.24 \text{ d}^{-1}$ ).

710 |       These growth rate variations are in broad agreement with the development of  
711 | blooms in these regions – in that the lowest biomass accumulation over the study period  
712 | occurred in the recirculation, with higher values over the plateau. In contrast, the model  
713 | suggests that the highest growth rates occurred in Group 4 coastal waters, where biomass  
714 | accumulation was only moderate, and found only moderate growth rates for the Group 5  
715 | Polar Front stations where a strong bloom was already underway at the time of sampling  
716 | (Fig. 2). [Unfortunately, it](#) is not currently possible to determine [why this misfit occurred,](#)  
717 | [and it is not really surprising given whether this reflects](#) the simplicity of the model [and or](#)  
718 | the complexity of the ecosystem dynamics. This provides a useful cautionary note that the

Formatted: Superscript

Formatted: Superscript

719 apparent growth rate variations have no real quantitative validity; at best they provide  
720 indicative information on the relative intensities of CO<sub>2</sub> assimilation across the Groups.  
721 Indeed, it is possible that the variations among the Groups results from other issues such  
722 as species metabolic differences, or light and trace element availability (as discussed in  
723 detail in the Methods section). Thus it is important to emphasize that the overall view of  
724 ecosystem responses developed in the Discussion section below does not depend only on  
725 these potential growth rate estimates from the <sup>13</sup>C-POC observations, but also draws on  
726 biomass accumulation rates from the POC concentrations, their distribution across size  
727 fractions, and other indicators as discussed below.

Formatted: Superscript

### 729 3.4 <sup>15</sup>N variations

730 Similarly to the carbon isotopes, we discuss the <sup>15</sup>N-PN variations relative to co-  
731 located <sup>15</sup>N-NO<sub>3</sub> values ( $^{15}\text{N-PN}_{\text{rs}} = ^{15}\text{N-PN} - ^{15}\text{N-NO}_3$ ), for the reasons outlined in the  
732 Methods (section 2.5.2). As shown in Fig. 4, almost all the phytoplankton dominated size  
733 fractions (5-20, 20-50, 50-210 μm) had <sup>15</sup>N-PN<sub>rs</sub> values that fall between the upper bound  
734 of production from nitrate ( $^{15}\text{N-PN}_{\text{rs}} = -4$ ) and the lower bound of production from  
735 ammonium ( $^{15}\text{N-PN}_{\text{rs}} = -8$ ). There was also a tendency across all Groups towards lower  
736 <sup>15</sup>N-PN<sub>rs</sub> in the smaller phytoplankton fractions; consistent with greater use of ammonium  
737 by smaller phytoplankton (Armstrong, 1999; Karsh et al., 2003). The largest zoo-plankton  
738 containing size fractions (210-300, 300-1000 μm) had higher <sup>15</sup>N-PN<sub>rs</sub> values, which  
739 presumably result from the relatively large (~3 ‰) trophic enrichment that occurs in many  
740 marine organisms (Michener and Schell, 1994; Wada and Hattori, 1978). While these  
741 general variations with size held for all Groups, there were significant differences. In  
742 particular, the Group 3 plateau stations had the lowest <sup>15</sup>N-PN<sub>rs</sub> values for the larger  
743 autotrophic size classes (20-50 and 50-210 μm).

744 Using the end-member mixing model (Methods section 2.5.2), we obtained the  
745 estimated community  $f$  ratios as shown in Fig. 5. The Group 3 plateau stations tended to  
746 have somewhat higher values ( $\sim 0.7$  vs.  $\sim 0.6$ ) than the Group 5 downstream Polar Front  
747 bloom stations (TEW-7, TEW-8, and F-S); although this was not true for the highest  
748 biomass station (F-L). As with the <sup>13</sup>C model growth rates, the Group 1 recirculation  
749 stations sampled early on the TNS transit were somewhat surprising in having relatively  
750 high values, though these were not observed on the later TEW transit or during the Group  
751 2 time series. Finally, the coastal stations had high *apparent*  $f$  ratios, including values that  
752 exceed 1 (pointing to limitations of the model). Importantly, these high values are driven  
753 by the relatively low <sup>15</sup>N-NO<sub>3</sub> values in these coastal waters, rather than by higher <sup>15</sup>N  
754 contents in their PON. The low <sup>15</sup>N-NO<sub>3</sub> values are a surprise given the relatively low  
755 nitrate concentrations in these coastal waters (Fig. 6), suggesting other processes are at  
756 work. Our observations are insufficient to explain this. One possibility is delivery of low  
757 <sup>15</sup>N nitrate from sedimentary nitrification, but this still leaves open the question of why  
758 recently formed PN does not track the overall nitrate pool isotopic composition. Reliance  
759 on the  $f$  ratios from these coastal stations is thus not advisable. In contrast, comparison of  
760 our offshore  $f$  ratios to incubation results (Fig. 5) shows similar values and excellent  
761 correlation ( $r^2=0.90$ ; provided the one very low incubation based  $f$  ratio at the HNLC  
762 station R2 is discounted).

763

### 764 3.5 Nutrient depletion estimates

765 Surface water nutrient concentrations provide an initial perspective on the efficiency of  
766 the biological pump. ~~Overall, the~~ surface nitrate concentrations ~~indicate were~~ lower  
767 ~~values~~ north than south of the Polar Front, but of course this may reflect longer term,  
768 ~~larger region~~ basin scale, controls on nitrate. Determination of the role of local recent

Formatted: Superscript

769 biological activity in nitrate depletion requires a much closer examination. Fig. 6 shows  
770 high spatial resolution maps of nitrate, temperature, and salinity obtained with the sensors  
771 operated continuously underway. Waters upstream from the plateau and south of the Polar  
772 Front were cold and saline with high nitrate concentrations, with these parameters  
773 reaching their highest values over the central plateau early in the voyage (near the Group 3  
774 KEOPS bloom reference station A3-1), with temperature less than 2°C, salinity greater  
775 than 33.9, and nitrate above 30  $\mu\text{M}$ . At the other extreme, Group 4 coastal waters had the  
776 lowest surface nitrates (below 10  $\mu\text{M}$ ), in association with very fresh (salinity <33.6) and  
777 relatively warm (>3.5°C) waters. The Group 5 waters downstream in the bloom that  
778 formed north of the Polar Front well to the east (near 74-75°E and the Group 5 stations  
779 TEW-7, -8, F-L and F-S), also had relatively low surface nitrates (15-20  $\mu\text{M}$ ) and low  
780 salinities (33.7-33.8), and were quite warm (>4 °C). In comparison, The Group 2  
781 recirculation feature had intermediate nitrate concentrations between the plateau, coastal,  
782 and downstream Polar Front plume conditions.

783         These conditions evolved over the course of the study, with decreases in surface  
784 nitrate values being particularly strong (reaching 6-8  $\mu\text{M}$  from winter conditions; Table 4)  
785 in regions of rapid biomass accumulation over the central plateau (especially along the  
786 plateau edge to the north of the A3 station) and in the bloom north of the Polar Front (near  
787 stations TEW-8, F-L, F-S). Low nitrate concentrations were also found in association with  
788 relatively low salinities to the southeast of the recirculation region, where the ship  
789 transited without station sampling. This appears to represent southward supply of waters  
790 from north of the Polar Front in association with its meandering (as also suggested by the  
791 satellite chlorophyll image sequences (Fig. 2 and animation in the Supplement, and by  
792 water parcel trajectories estimated from drifters and satellite altimetry; d'Ovidio et al.,  
793 2014). This process also appears to have driven warming and freshening in the

794 recirculation over time. Thus nitrate budgets require partitioning of temporal changes  
795 driven by both hydrology and biology.

796 To separate local biological nitrate depletion from hydrological controls, we  
797 examined nitrate depletions in surface waters relative to estimates of initial winter nitrate  
798 concentrations for each station, as estimated from CTD profiles. We considered  
799 integrations to two different depths: (a) the frequently used choice ~~(e.g.~~ (e.g. Arrigo et al.,  
800 1999; Sweeney et al., 2000) of the depth of the remnant winter water temperature  
801 minimum ( $T_{\min}$ -depth), and (b) shallower depths based on a threshold increase in salinity  
802 of 0.05 ( $S_{\text{threshold}}$ -depth). This second choice was motivated by the presence of significant  
803 salinity gradients above the  $T_{\min}$ -depth (examples are shown in Fig. 7), particularly in  
804 waters near and north of the Polar Front, suggesting either that the most recent winter  
805 mixing was not as deep as previous years, or that horizontal mixing had brought fresher  
806 waters over the top of the  $T_{\min}$ , and thus in either case that nitrate depletion between the  
807  $T_{\min}$ -depth and  $S_{\text{threshold}}$ -depth was not attributable to ~~recent consumption~~ local biological  
808 processes. ~~Note that each of these nitrate depletion metrics reflects the sum of export~~  
809 ~~since stratification and the current standing stock, which may make a contribution to future~~  
810 ~~export (at some unknown discounted rate owing to heterotrophic loss).~~

811 The two nitrate depletion metrics give differing views of the contributions to  
812 export from the different community Groups (as summarized in Fig. 8). Estimates based  
813 on the  $T_{\min}$  approach were much higher than those from the  $S_{\text{threshold}}$  approach, because the  
814  $T_{\min}$ -depth was generally deeper and had higher nitrate than the  $S_{\text{threshold}}$ -depth (Table  
815 24). ~~The  $T_{\min}$  approach also yielded more widely varying results within a Group.~~ The  $T_{\min}$   
816 approach ~~and~~ suggested that the greatest depletion occurred ~~for in~~ in the downstream plume  
817 ~~of Kerguelen island coastal waters that formed the bloom~~ to the north of the Polar Front.  
818 In contrast, the  $S_{\text{threshold}}$  approach identified the highest seasonal nitrate depletion as

819 occurring over the central plateau, with somewhat lower values in the recirculation feature,  
820 followed by the Polar Frontal bloom and the reference station. These methodological  
821 differences were even larger for the silicic acid depletions (Fig. 8). This analysis  
822 underlines the importance of appropriate winter nitrate (and silicic acid) surface nitrate  
823 concentration estimates to the assignment of export magnitudes.

824 We believe the  $S_{\text{threshold}}$  approach is the most appropriate given the observed  
825 salinity stratification, especially for the relatively weak subsurface thermal stratification  
826 observed in the Group 5 stations near the Polar Front, where its choice makes the most  
827 significant difference from estimates based on the  $T_{\text{min}}$  approach. This is because the high  
828 biomass layer found in these Polar Frontal sites is in this shallow salinity-defined layer,  
829 and because the Fe fertilization of these waters is recent as shown by their short transit  
830 time of ~ 2 weeks since crossing the plateau as determined from both altimetry and drifter  
831 releases (d'Ovidio et al., 2014; Park et al., 2014). Thus attribution of nutrient depletion  
832 below the depth of the  $S_{\text{threshold}}$  to local iron fertilized biomass production is not

833 warranted.~~We believe the  $S_{\text{threshold}}$  approach is the most appropriate given the observed~~  
834 ~~salinity stratification, especially for the relatively weak subsurface thermal stratification~~  
835 ~~observed in the Group 5 stations near the Polar Front. Both~~ For all the Groups, both the  
836  $T_{\text{min}}$  and  $S_{\text{threshold}}$  based nitrate depletions are relatively small as percentages of the initial  
837 upper water column inventories (2-18%; Table 4). This reflects the early seasonal  
838 sampling, as well as a significant extent of recycling via nitrification (Dehairs et al.,  
839 2014; Lasbleiz et al., 2014). Fractional depletions of silicate were higher (3-53%; ~~data but~~  
840 ~~not values shown in~~ Table 4b), consistent with the results of the autumn KEOPS  
841 expedition which revealed low nitrate removal but near complete Si depletion (Mosseri et  
842 al., 2008). Finally, Note we note that we could not estimate export for the Group 4

Formatted: Font: 12 pt, Font color: Auto

Formatted: Indent: First line: 1.27 cm

Formatted: Font: 12 pt, Font color: Auto

Formatted: Font: 12 pt, Font color: Auto

843 Kerguelen Island coastal stations because neither the  $T_{\min}$  nor the  $S_{\text{threshold}}$  approaches were  
844 compatible with their shallow water columns).

845 Our preferred  $S_{\text{threshold}}$  nitrate depletion estimate can be further refined by removal  
846 of the standing stock of other nitrogen forms produced by the ecosystem (ammonium, urea,  
847 dissolved organic nitrogen, particulate nitrogen) to give a better estimate of N export from  
848 surface waters. PN dominated these stocks, with concentrations up to 5  $\mu\text{M}$  (Lasbleiz et  
849 al., 2014)), in contrast to ammonium, nitrite, and surface enhancements of DON (i.e. the  
850 fresh component) with concentrations below 1  $\mu\text{M}$  (Blain et al., 2014;Dehairs et al., 2014).  
851 Subtracting PN stocks (integrated to 200m depth (Lasbleiz et al., 2014) suggests that for  
852 many stations about half of the consumed nitrate has been exported and about half remains  
853 in the water column (Table 4).

854 A few stations exhibited negative N export estimates, because of higher PN stocks  
855 than their nitrate depletion estimates (Table 4). This could arise from either  
856 underestimation of nitrate depletions owing to entrainment of subsurface waters (an effect  
857 that can halve nutrient depletion estimates under conditions of weak water column  
858 stratification and strong winds; (Wang et al., 2003)), or horizontal interleaving of  
859 relatively undepleted water parcels with relatively PN rich waters. Notably the largest  
860 excesses of PN stock over nitrate depletions occurred at stations located close to fronts  
861 (TEW-3 and F-S).

862 Viewed at the Group level, the nitrate depletions and N export estimates (Fig. 8)  
863 provide very useful insights. [Firstly, given the uncertainties regarding the estimation of  
864 nutrient depletions from the profiles, it could be argued that the most robust conclusion is  
865 that all the Groups exhibit similar depletions, with roughly half of the N uptake exported  
866 and half remaining as accumulated biomass. This is consistent with the growth estimates  
867 of roughly one doubling every 3 days and the satellite biomass observations indicating](#)

868 | [slower doubling approximately each week. Looking into more detail, and Focusing](#)  
869 | [focusing](#) on the salinity threshold approach, [we seesuggests](#) that the highest nitrate  
870 | depletions occurred for the Group 3 plateau stations, with significantly lower values in the  
871 | Group 1 and Group 2 recirculation stations (Fig. 8 middle panel). However, the larger  
872 | standing stock of PN biomass over the plateau means that the export up to the time of  
873 | sampling was only slighter higher than in the Group 1 and 2 recirculation stations. This  
874 | aspect is even stronger for the Si budgets, with the export of Si higher for Groups 1 and 2  
875 | than over the plateau in Group 3, emphasizing the retention of N in comparison to Si  
876 | during export.

877 | Another interesting insight is that, in comparison to the Group 3 plateau stations,  
878 | nitrate depletion and export are much lower in the Group 5 Polar Frontal bloom stations.  
879 | Considering the  $S_{\text{threshold}}$ -depths (Table 4), and the associated Si depletion and export  
880 | results (Fig. 8), helps understand why the Polar Frontal bloom [produces-produced](#) less  
881 | nitrogen depletion and export than the plateau bloom. Firstly, the Polar Frontal bloom  
882 | depletion is a shallow feature compared to that over the plateau (Fig. 7), secondly a much  
883 | greater proportion of the assimilated nitrogen is still present as standing stock (Fig. 8  
884 | bottom panel), and thirdly, there is some suggestion that more nitrogen than silicon is  
885 | retained as standing stock (as a portion of depletion; compare the Fig. 8 middle and bottom  
886 | panels). [Of course observation of these variations in spring does not mean that they would](#)  
887 | [have persisted into summer, and it is possible that over the full season the extent of](#)  
888 | [nutrient depletion was significantly different then observed during the KEOPS2 shipboard](#)  
889 | [campaign, either towards homogeneity across the region or towards larger variations.](#)

890

#### 891 | **4. Discussion**



892 Our overall interest is to understand community responses to iron fertilisation, with  
893 a particular focus on ecosystem control of nutrient depletion and carbon export. We  
894 expect this response to vary as a function of iron inputs, but also possibly with time since  
895 fertilisation and its persistence (as a result of cascading trophic effects), and time of year  
896 (as a result of strong seasonality of the physical and biological background). Specific  
897 probable seasonal modulators of the response to iron include insolation, stratification, and  
898 the abundance of organisms with life cycles that resonate at the seasonal scale, e.g. larger  
899 zooplankton. In the following sections, we summarize the structure and function  
900 variations, relate them to temporal settings (as developed in the Methods section), and  
901 compare them to our estimates of nitrate (and silicic acid) depletion from surface waters as  
902 a proxy for carbon export.

903

#### 904 **4.1 Overview of community structure and function variations**

905 Our size-fractionated chemometric parameters for microbial ecosystem structure  
906 and function identified significant differences among the various environments sampled by  
907 the KEOPS2 program. The upstream HNLC reference station (R2) displayed low  
908 phytoplankton abundance, relatively high BSi/POC ratios, slow growth rates (as indicated  
909 by [both](#) strong discrimination against  $^{13}\text{C}$  uptake ([this work](#)) and [slow growth rates](#)  
910 [measured in deckboard incubations](#) (Cavagna et al., 2014)), ~~and its~~  $^{15}\text{N}$ -PN values  
911 ~~suggesting~~ ~~suggested~~ that growth was predominantly on nitrate, ~~(although this result must~~  
912 ~~be viewed with caution since it differs from the~~ [surprisingly](#) low  $f$  ratio obtained by  
913 ~~incubation~~ (Cavagna et al., 2014). These characteristics are consistent with its selection  
914 as a HNLC reference, but the total integrated biomass was higher than the lowest values  
915 seen in Southern Ocean HNLC waters and mesopelagic Ba levels indicated POC  
916 remineralization, possibly indicating a low-level early production event (Jacquet et al.,

917 2014;Lasbleiz et al., 2014) as a result of a small degree of Fe fertilisation, possibly from  
918 particulate Fe inputs from the nearby Leclaire Rise (van der Merwe et al., 2014).

919 The moderate iron fertilisation of the recirculation feature downstream from the  
920 plateau (stations in Groups 1 and 2) increased <sup>13</sup>C model growth rates (relative to the  
921 HNLC reference station R2) by ~0.02 to 0.04 d<sup>-1</sup> (Fig. 5) and biomass ~2-fold (increasing  
922 from ~50% to 4-fold over time; Fig. 3), particularly in the larger phytoplankton size  
923 fractions (20-50 and 50-210 µm). There was no systematic change in BSi/POC ratios,  
924 with some stations showing lower values consistent with relief of iron limitation, but  
925 others showing higher values. Whether this resulted primarily from changes in species or  
926 the presence of empty frustules is unclear, although the analysis of depletions and standing  
927 stocks suggests loss of empty frustules (as did earlier work during KEOPS; (Mosseri et al.,  
928 2008)). This may reflect varying levels of low production (Cavagna et al., 2014) coupled  
929 closely to export, as well as the possibility that production was in part limited by  
930 variations in mixed layer depth (Lasbleiz et al., 2014). The <sup>15</sup>N-PN observations indicated  
931 growth primarily on nitrate (as at the HNLC reference station).

932 Both of the more strongly iron fertilised offshore regions (the Group 3 central  
933 plateau and the Group 5 Polar Front bloom, Table 1.) exhibited increased <sup>13</sup>C model  
934 growth rates in comparison to HNLC waters (elevated by ~0.05 d<sup>-1</sup>), but their community  
935 structures were quite different (emphasizing caution regarding the <sup>13</sup>C model growth rates,  
936 although the incubation results also indicated increased growth rates; (Cavagna et al.,  
937 2014)). The plateau stations exhibited most of their enhanced biomass in the largest  
938 phytoplankton size fraction (50-210 µm); whereas Polar Frontal biomass increases were  
939 dominated by the next smaller size (20-50 µm). This was also true for the very strongly  
940 Fe fertilized Group 4 coastal stations where <sup>13</sup>C model growth rates were even more  
941 elevated (by 0.1 to 0.19 d<sup>-1</sup> above the HNLC reference). Use of ammonium vs. nitrate (as

Formatted: Superscript

Formatted: Superscript

Formatted: Superscript

942 | [estimated from both natural abundance  \$^{15}\text{N}\$  values in this work and tracer  \$^{15}\text{N}\$  uptake](#)  
943 | [incubations by Cavagna et al., 2014](#)), was also different between the plateau and  
944 | downstream Polar Frontal blooms, with the plateau stations using a greater proportion of  
945 | nitrate.

946

#### 947 **4.2 Links between community structure and export**

948 | Overall, one of the most important outcomes of our results regarding export (presented  
949 | in section 3.5 and Fig. 8) is that surface biomass is not a good guide to the history of  
950 | export, i.e. the low biomass recirculation feature exhibited as much export as from the  
951 | higher biomass Polar Front or Plateau blooms. This same conclusion was reached on the  
952 | basis of sparse sediment trap deployments at 200 m depth (Laurenceau et al., 2014) and  
953 |  $^{234}\text{Th}$  depletions in surface waters, which identified the recirculation feature as having the  
954 | highest C exports of all regions (Planchon et al., 2014).

955 | The cause of the low export, at 200m depth, from the Polar Front bloom (Group 5  
956 | downstream stations) may in part be the shallowness of its high biomass surface layer  
957 | (only ~ half that of the recirculation feature and plateau; (Lasbleiz et al., 2014; Laurenceau  
958 | et al., 2014)), allowing for more remineralisation before export through the 200m depth  
959 | horizon.

960 | The cause of the high export from the low biomass recirculation feature is less easy to  
961 | understand – it suggests that production (also found to be moderately high in these waters  
962 | compared to the other regions; (Cavagna et al., 2014)) and export have been in close  
963 | balance in these waters. This is a phenomenon often found in association with small  
964 | phytoplankton dominated communities, and attributed to tight coupling with small grazers  
965 | (Boyd and Newton, 1999; Cullen, 1995). Our observations show that this tight coupling  
966 | also persisted as very large, moderately to heavily silicified diatoms (Fig. 3) became

967 dominant. This suggests that tight coupling may have also been achieved for the larger  
968 phytoplankton. Notably there were abundant large herbivorous zooplankton in the  
969 recirculation region (Carlotti et al., 2014), and large fecal pellets as well as diatom  
970 aggregates were important contributors to export, based on observations in polyacrylamide  
971 gel filled sediment traps (Laurenceau et al., 2014). In making these comparisons among  
972 the station Groups, it is of course important to remember that our observations of nutrient  
973 depletion and export apply only at the this early spring observation time, and the  
974 subsequent evolution of the different water parcels may lead to different outcomes when  
975 averaged over the full annual cycle.

#### 977 **4.3 Influence of fertilisation time and persistence on ecosystem responses**

978 As developed in the Methods section, we consider four possible relative indices for  
979 the nature of the Fe fertilization and the overall ecosystem responses:

980 i. Intensity of Fe fertilisation (lowest to highest):

981 *recirculation feature < plateau  $\approx$  Polar Front plume << coastal stations*

982 ii. Elapsed time since Fe fertilisation and its persistence (most recent to oldest):

983 *Polar Front plume < recirculation feature  $\approx$  plateau < coastal stations*

984 iii. Magnitude of biomass accumulation (lowest to highest, at end of voyage):

985 *recirculation feature < coastal stations < plateau  $\approx$  Polar Front plume*

986 iv. Elapsed time since initiation of biomass accumulation (most recent to oldest):

987 *recirculation feature < Polar Front plume  $\approx$  plateau << coastal stations*

988 If we put aside the coastal stations, where depletion and export could not be estimated,  
989 we can ask which of these might explain why the recirculation feature achieved high  
990 export in comparison to its low to moderate biomass and low to moderate intensity of iron  
991 fertilisation. Index (ii) emerges as the most likely candidate – the recirculation feature

Formatted: No underline

992 receives low intensity ongoing iron fertilisation as a result of the recirculation of waters  
993 along the Polar Front and into it from the northeast (d'Ovidio et al., 2014), with possible  
994 augmentations from shallow Ekman transport from the nearby Kerguelen shelf (d'Ovidio  
995 et al., 2014;Sanial et al., 2014). This is a fascinating possibility, because it suggests  
996 ecosystems are modulated differently by persistent as opposed to punctual inputs of Fe.

997 ~~Index-Indices (i) and~~ (iv) also lists the recirculation as an end-member, but it seems  
998 unlikely that low Fe levels or lower biomass ~~is of itself aare~~ drivers of low-high export,  
999 given that many studies of export have found positive correlations with biomass, though  
1000 with significant modulation by community structure, e.g. (Boyd and Newton, 1995;Boyd  
1001 and Newton, 1999;Boyd and Trull, 2007;Buesseler, 1998;Buesseler et al., 2001;Buesseler  
1002 et al., 2007).

1003 Do any of these indices also provide insight on why the community differs  
1004 between the two strongly iron fertilised regions (the central plateau vs. the downstream  
1005 Polar Front)? For size structure, none of the time perspectives (indices ii-iv) appears to  
1006 help – the plateau and recirculation features with their dominance by very large diatoms  
1007 (vs. the more balanced size structure of the coastal and downstream Polar Front bloom) do  
1008 not fall appropriately along any of the time spectrums of these three ‘clocks’. To the  
1009 extent that the intensity of iron fertilisation (index i) may have been higher in both coastal  
1010 and Polar Front waters than over the plateau, despite similar current Fe levels (see the  
1011 Methods section for discussion), this could provide an explanation, but it would imply that  
1012 more Fe produces communities with smaller cells and thus be counter to the results of  
1013 artificial iron experiments (Boyd et al., 1999;Boyd et al., 2007). This leaves us with the  
1014 strong possibility that the community structure differences between the plateau and Polar  
1015 Front regions derive in part from other factors beyond levels, timing, or persistence of iron  
1016 fertilisation.

1017

1018 **5. Conclusions**

1019 A complex mosaic of phytoplankton blooms forms in response to natural iron fertilisation  
1020 from the Kerguelen plateau. Community structure variations in the downstream waters  
1021 appear to have multiple influences, including the intensity and persistence of iron  
1022 fertilisation, the progress of biomass accumulation, and possibly whether they were  
1023 sourced from plateau vs. coastal waters. These differences developed even though  
1024 phytoplankton growth rates appeared to increase more directly with the level of iron  
1025 availability, pointing to additional influences from trophodynamics. These community  
1026 effects strongly decoupled levels of surface biomass from levels of particle export to the  
1027 ocean interior over the timescales of spring bloom development studied here.

1028

1029

1030 **Tables**

1031 **List of Tables**

1032 Table 1. Station Groups

1033 Table 2. Chemometric results for size-fractionated particles

1034 Table 3. Particle size parameters used in the growth rate model

1035 | Table 4a. Surface mixed layer ~~nutrient-N~~ depletion and export estimates

1036 | [Table 4b. Surface mixed layer Si depletion and export estimates](#)

1037

1038

1039

1040

1041

1042 **Figure Captions**

1043 | Figure -1. Map of KEOPS-2 station locations. The Kerguelen and Heard islands mark the  
1044 northern and southern end of the central plateau (bathymetry in meters). The Polar Front  
1045 jet that passes through the mid-depth channel south of Kerguelen Island is shown as a bold  
1046 line. Full ocean depth flows of the Antarctic Circumpolar Current pass to the north of  
1047 Kerguelen Island in association with the Subantarctic Front and to the south of Heard  
1048 Island in the Fawn Trough. This latter flow follows the eastern slope of the plateau  
1049 northwards to bring cold waters into a bathymetrically trapped quasi-stationary  
1050 recirculation feature (d'Ovidio et al., 2014; Park et al., 2014a). Waters over the central  
1051 plateau are also carried into this region. During the initial survey, the TNS transect was  
1052 sampled first (south to north) and then the TEW transect (west to east). The E stations  
1053 were designed to provide a Lagrangian temporal sequence in the recirculation region  
1054 (including some to the east and west of its centre), with interspersed visits to the HNLC  
1055 reference station (R2); the region of high biomass near and north of the Polar Front (F-L  
1056 and F-S), and the central plateau bloom station (A3) previously studied in autumn 2005 by  
1057 the KEOPS project. Two additional stations (G1, G2) carried out for high volume  
1058 geochemical tracer studies and provided additional plateau and coastal samples,  
1059 respectively. The stations are colour coded into 5 Groups as shown on the map (QGIS) and  
1060 detailed in Table 1.

1061  
1062 Figure 2. Temporal development of the Kerguelen bloom. Successive images of surface  
1063 chlorophyll distributions (NASA MODIS-Aqua; SSALTO/DUACS 1 km daily product)  
1064 show the bloom development. Image date 28 October: most stations of the initial survey  
1065 downstream of Kerguelen Island (TNS 1-10, TEW 1-6), the HNLC reference station (R2,  
1066 upstream) and the first visit to the KEOSP1 plateau reference station (A3-1 at the southern



1067 end of the TNS transect) were sampled before any significant biomass accumulation had  
1068 occurred. Image date 06 November: The developing downstream Polar Front bloom (TEW  
1069 7, TEW 8, F-L, F-S) was sampled early in its development, and the recirculation visited a  
1070 second time (E2). Image date 11 November: the now well developed central plateau  
1071 bloom was sampled (G1; E4-W) along with also blooming coastal waters (G2). Two more  
1072 visits to the still low biomass recirculation were also completed (E3 and E4-E). Image  
1073 date 18 November: the plateau bloom was re-sampled as it began to fade (A3-2 and E4-  
1074 W2), along with the final recirculation station (E5). Bathymetry is shown by contours at  
1075 1000, 2000, and 3000 m depths. A full annual animation of the phytoplankton bloom  
1076 evolution is available in the [supplement](#) [Supplement](#).

1077

1078 Figure 3. Surface water total and size-fractionated POC and BSi concentrations.

1079 Top row: total POC and BSi concentrations for the identified station Groups (see Table 1);  
1080 individual stations in each group are in chronological order from left to right. Middle row:  
1081 POC size distribution spectra, i.e. concentrations normalised by dividing by the width of  
1082 the size fraction (i.e. division by 4 for the 1-5  $\mu\text{m}$  fraction); dotted lines provide visual  
1083 guides and reveal little variation among groups for the smallest particles, and largest  
1084 variations in the intermediate size fractions. Bottom row: BSi/POC ratios; grey band  
1085 indicates approximate range of values for extant diatoms, with higher values possibly  
1086 indicative of higher iron stress.

1087

1088 Figure 4. Isotopic variations in the size-fractionated particles.

1089 Top row:  $^{13}\text{C}$ -POC values relative to  $^{13}\text{C}$ -DIC values; dotted line shows the lowest values  
1090 for the intermediate, autotrophic, size fractions samples as observed at upstream Fe poor  
1091 reference station (R2). Bottom row:  $^{15}\text{N}$ -PON values relative to co-located  $^{15}\text{N}$ - $\text{NO}_3^-$

1092 values; grey band indicates values expected for phytoplankton that grow exclusively on  
1093 nitrate.

1094

1095 Figure 5. Isotopic chemometric estimates of growth rates and f-ratios

1096 Top row: Growth rates based on the supply vs. demand  $^{13}\text{C}$  isotopic fractionation model  
1097 (summed across the 4 smallest particle size fractions). Estimates from a limited set of  $^{13}\text{C}$   
1098 tracer uptake incubations are shown as darker bars (measured at varying light levels and  
1099 integrated to the mixed layer depth light level; (Cavagna et al., 2014)). Bottom row:  $f$   
1100 ratios, i.e. the fraction of total nitrogen nutrition provided by nitrate, based on the  $^{15}\text{N}$   
1101 ammonium and  $^{15}\text{N}$  nitrate end-member mixing model (summed across 4 smallest particle  
1102 size fractions). Estimates from a limited set of  $^{15}\text{N}$  tracer uptake incubations are shown as  
1103 darker bars (Cavagna et al., 2014).

1104

1105 Figure 6. High resolution distributions of surface water properties from continuous sensor  
1106 measurements.

1107 Top to bottom: ship trajectory as revealed by dates of sampling; nitrate concentrations  
1108 (from [ISUS UV-ultra-violet](#) spectrometry), temperature, and salinity, [ISUS](#)). Stations at  
1109 the ends of the trajectories are indicated to aid in co-location with the lower resolution  
1110 station sampling map (Fig. 1).

1111

1112 Figure 7. Example profiles of temperature, salinity, nitrate concentrations, and nitrate  
1113 isotopic compositions. Top row: Group 3 central plateau station A3-2. Middle row: Group  
1114 5 downstream Polar Front station F-L. Bottom row: Group 5 Subantarctic station TNS-1.  
1115 Depths of the remnant winter water  $T_{\min}$  mixed layer depth ( $T_{\min}$ -depth; solid line) and  
1116 salinity stratification mixed layer depth ( $S_{\text{threshold}}$ -depth; dotted lines) are shown. These

1117 depths define our two approaches for the calculation of depth integrated nitrate and silicate  
1118 depletions (Table 4; Fig. 8).

1119

1120 Figure 8. Nitrogen and silicon depletion and export estimates

1121 Top row: nitrate (light bars) and silicate (dark bars) depletions from the  $T_{\min}$  winter

1122 concentration method. Middle row: nitrate (light bars) and silicate (dark bars) depletions

1123 from the  $S_{\text{threshold}}$  winter concentration method. Bottom row: N (light bars) and Si (dark

1124 bars) export, as estimated from the  $S_{\text{threshold}}$  depletion method, after accounting for the PN

1125 and BSi standing stocks integrated to 200m (Table 4; (Lasbleiz et al., 2014)). Group 4

1126 coastal stations are not shown because CTD casts could not define winter values. Negative

1127 export values are not plotted ([see Table 4 and text](#)). Groups 1, 2, 3 and 4 are coloured as

1128 in Fig. 1 and are ranked from left to right with temporal order within each group.

1129

1130

1131 **Appendix A: Chemical and isotopic analyses**

1132 **A1 Particle collection**

1133 The ship supply collected water from ~7m depth via a 10 cm diameter plastic hose  
1134 extended through a vertical stainless-steel stand-pipe protruding ~1 m below the ship's  
1135 forward hull. A sealed rotary propeller pump drew the supply through a 1000 µm nylon  
1136 cylindrical pre-filter and distributed it via a manifold at more than 50 L min<sup>-1</sup>, with most  
1137 water returned over the side. This pre-filter was cleaned before each sample, and then a  
1138 manifold valve was opened to supply a smaller flow of 8-10 L min<sup>-1</sup> through our small  
1139 volume bulk particle and large volume sequential filtration systems. The large volume size  
1140 fractionation system passes the water through a 47 mm diameter 1000 µm screen (to  
1141 remove any large particles that managed to pass through the pump pre-filter at higher flow  
1142 rates), followed by 142 mm diameter Nitex nylon screens (300, 210, 50, 20, and 5 µm  
1143 mesh sizes) and a final 142 mm diameter QMA quartz fibre filter (1 µm nominal pore size,  
1144 Sartorius). The small volume bulk enclosed sample system rapidly fills a precisely known  
1145 ~1 L volume and low pressure filters it through a QMA quartz filter (muffled and pre-  
1146 loaded under clean conditions into in-line filter holders). Quartz filters were used in  
1147 preference to glass to minimize <sup>234</sup>Th backgrounds and to give better combustion  
1148 characteristics during elemental and isotopic analysis. The flow path allowed a larger flow  
1149 rate through the larger meshes (Table 2). The very minor amounts of material on the 1000  
1150 µm screen were not analysed. Particles on the other nylon screens were immediately  
1151 resuspended (1 µm filtered seawater from the sampling location) and refiltered onto 25  
1152 mm diameter, 1.2 micron pore size silver membrane filters (Sterlitech) and, along with the  
1153 QMA filter (Sartorius T293), were dried at 60°C. Following drying, the particles were  
1154 examined under stereo-microscopy onboard the ship at magnification up to 50x, and then

1155 analysed non-destructively onboard for  $^{234}\text{Th}$  activities (Planchon et al., 2014). All other  
1156 analyses were carried out in the Hobart laboratories.

1157

## 1158 **A2 Particle analyses**

1159 Biogenic silica (BSi), Particulate organic carbon (POC), and particulate nitrogen (PN),  
1160  $\delta^{13}\text{C}$ -POC, and  $\delta^{15}\text{N}$ -PN analyses were carried out in Hobart. For BSi, a single 5mm  
1161 diameter punch of the silver filters was analysed using an approach used previously for  
1162 Southern Ocean samples (Queguiner, 2001). The biogenic silica was dissolved by adding  
1163 4mL of 0.2M NaOH and incubating at 95°C for 90 minutes. Samples were then rapidly  
1164 cooled to 4°C and 1mL of 1M HCl was added. Thereafter samples were centrifuged at  
1165 1880 x g for 10 minutes and the supernatant was transferred to a new tube and diluted with  
1166 artificial seawater (36 g L<sup>-1</sup> NaCl). Biogenic silica concentrations were determined by  
1167 spectrophotometry using an Alpkem model 3590 segmented flow analyser and following  
1168 USGS Method I-2700-85 with these modifications: ammonium molybdate solution  
1169 contained 10g L<sup>-1</sup> (NH<sub>4</sub>)<sub>6</sub>Mo<sub>7</sub>O<sub>24</sub>, 800µl of 10% sodium dodecyl sulphate detergent  
1170 replaced Levor IV solution, acetone was omitted from the ascorbic acid solution, and  
1171 artificial seawater was used as the carrier solution. Biogenic silica standard concentrations  
1172 were 0 µM, 28 µM, 56 µM, 84 µM, 112 µM and 140 µM. Standard curves across all runs  
1173 had an average slope of 48 438 ± 454 (1 s.d. n=4). The mean concentration of repeated  
1174 check standards (140 µM) was 139.85± 0.31 µM (n=68). The average blank value was  
1175 0.009 ± 0.006 µmoles punch<sup>-1</sup> (1 s.d. n=5), equating to 0.08% of the mean of 50 µM  
1176 fraction samples (highest concentrations) and 1.22% of the mean of 300 µM fractions  
1177 (lowest concentrations).

1178 For the POC and PN analyses, 3 x 5mm punched sub-samples of the 25 mm diameter  
1179 silver membrane filters were placed in acid-resistant silver capsules (Sercon SC0037),

1180 treated with two 10  $\mu$ L aliquots of 2N HCl (and 2 x 20  $\mu$ L for the bulkier QMA filter sub-  
1181 samples, 5 x 5mm punches) to remove carbonates (King et al., 1998), and dried at 60  $^{\circ}$ C.  
1182 A first set of sub-samples was analysed for POC and PN concentrations by combustion of  
1183 the encapsulated samples in a Thermo-Finnigan Flash 1112 elemental analyser with  
1184 reference to sulphanilamide standards in the Central Sciences Laboratory of the University  
1185 of Tasmania. Precision of the analyses was  $\sim$ 1 %, but the overall precision was limited to  
1186 5-10 % by the sub-sampling of the filters that often had patchy or uneven coverage. Based  
1187 on the POC and PN results, a third set of sub-samples was punched for isotopic analyses  
1188 with the number of punches adjusted to ensure similar voltages within the dynamic range  
1189 of the spectrometer.

1190  $\delta^{13}\text{C}$ -POC and  $\delta^{15}\text{N}$ -PN on the silver filters were analysed separately using a Fisons  
1191 NA1500 Elemental Analyser coupled via a Con-flow IV interface to a Finnigan Delta  
1192 V<sup>PLUS</sup> isotope ratio mass spectrometer at CSIRO Marine and Atmospheric Research with  
1193 separate oxidation and reduction columns installed. For the QMA filters, a Flash 2000  
1194 EA1112 HT Thermoscientific was fitted with a single combined oxidation/reduction  
1195 column with dead spaces minimised for improved precision at  $<20\mu\text{g N}$ . During all  $^{15}\text{N}$   
1196 analyses,  $\text{CO}_2$  was removed using a sodium hydroxide scrubber (self-indicating Ascarite 2,  
1197 Thomas Scientific) to avoid  $\text{CO}^+$  interference at  $m/z$  29 and 28 (Brooks et al., 2003). The  
1198  $\delta^{15}\text{N}$  and  $\delta^{13}\text{C}$  isotopic compositions are expressed in delta notation vs. atmospheric  $\text{N}_2$   
1199 and the VPDB standard, respectively. Standardization was by reference to  $\text{CO}_2$  and  $\text{N}_2$   
1200 working gases injected before and after each sample, with normalization to solid reference  
1201 materials inserted (along with blank cups) after each 6 samples. For  $\delta^{13}\text{C}$ , the solid  
1202 standards were NBS-22 oil (RM8539, -29.73 ‰) and NBS-19 (limestone, RM8544,  
1203 +1.95 ‰), and casein (Protein Standard OAS B2155 batch 114859, Elemental  
1204 Microanalysis,  $\delta^{13}\text{C}$  +5.94 and  $\delta^{15}\text{N}$  -26.98). For  $\delta^{15}\text{N}$ , the solid standards were IAEA-N1

1205 (ammonium sulphate, RM8547, +0.43‰) and IAEA-N3 (potassium nitrate, RM8549,  
1206 +4.72 ‰) and casein (as above). Based on replicate analyses of these standards the  
1207 estimated precisions were typically 0.1‰ or 1 standard deviation for both  $\delta^{13}\text{C}$  (n=15) and  
1208  $\delta^{15}\text{N}$  (n=20).

1209 Sample replicates generally had comparable precisions to the reference materials,  
1210 but filters with patchy coverage had lower precision (0.3‰ in the worst cases, presumably  
1211 reflecting isotopic heterogeneity within the size fractions). In addition, a small correction  
1212 of  $<+0.4\text{‰}$  was made to the QMA filter results after indirect [measurement estimation](#) of  
1213 the blank ([Avak and Fry, 1999](#))  $\delta^{13}\text{C} = -29.6$  ([Avak and Fry, 1999](#)), at ~10% of the  
1214 sample signal strength ([Avak and Fry, 1999](#)). Procedural blanks were measured by passing  
1215 1 litre of seawater through the onboard pumping system and subsequent processing in  
1216 parallel to the samples, and yielded negligible amounts of POC and PN (<1% of typical  
1217 samples), and with ratios close to those of the samples, and no correction was applied.

1218

### 1219 **A3 Dissolved component analyses**

1220 Underway nitrate concentrations were mapped using an ultra-violet nitrate sensor  
1221 (ISUS V3, Satlantic), calibrated 3 times during the voyage against sea water nitrate  
1222 standards (~15, 20, 25, 30  $\mu\text{M}$ ), with additional comparisons to nitrate samples collected  
1223 from the underway supply at every station sampled for particle analyses, yielding  
1224 precision of ~1.5  $\mu\text{M}$ . Nitrate concentrations for these samples and the CTD-Niskin bottles  
1225 were measured onboard using a segmented flow spectrometric autoanalyser, with  
1226 precision of ~0.1  $\mu\text{M}$ . The N and O isotopic compositions of dissolved nitrate were  
1227 measured via its bacterial conversion to nitrate to nitrous oxide followed by isotope ratio  
1228 mass spectrometry at the Vrije Universiteit Bruxelles, with precision of approximately 0.2‰

1229 for  $^{15}\text{N}\text{-NO}_3$  and of 0.4‰ for  $^{18}\text{O}\text{-NO}_3$  (further analytical details are provided in Dehairs et  
1230 al., 2014).

1231 Samples for measurement of the carbon isotopic composition of dissolved inorganic  
1232 carbon were collected in 10mL Exetainer vials, with airtight septa, by filling the tubes  
1233 from QMA filtered ( $\sim 0.8 \mu\text{m}$ ) underway supply and preserving them by addition of 20 $\mu\text{L}$   
1234 of saturated mercuric chloride. 1mL aliquots were withdrawn and injected into acid  
1235 washed, helium flushed Exetainer tubes. 100 $\mu\text{L}$  of ortho-phosphoric acid (99%, Fluka)  
1236 was injected and the headspace equilibrated at 25°C for 18 hours (modification of Assayag  
1237 et al., 2006). Solid NBS19  $\text{CaCO}_3$  (200 to 230 $\mu\text{g}$ ,  $\delta^{13}\text{C}=+1.98$ ,  $n=10$  standard deviation  
1238 0.02), and bulk quality assurance sediment trap material (1200 $\mu\text{g}$ , 12.9%  $\text{CaCO}_3$ ,  
1239  $\delta^{13}\text{C}=+2.9$ ), was weighed into smooth wall tin capsules (5x5.5mm SC1190, Sercon) and  
1240 lowered into the Exetainer tubes, purged, then 1mL of DIC free sea water added before  
1241 proceeding as for the samples. Blank, standard and sample headspaces (one standard after  
1242 each 5 samples) were sampled using a Finnigan GasBench2 (ThermoScientific) fitted with  
1243 a 100 $\mu\text{L}$  sample loop. The headspace gases from the Gas Bench were analysed  
1244 (continuous flow) by the DeltaV<sup>Plus</sup> isotope ratio mass spectrometer and Isodat 3 software  
1245 at CSIRO Marine and Atmospheric Research.

1246

1247

1248



1249 **The Supplement related to this article is available**  
1250 **online at doi:10.5194/bgd-11-13841-2014 supplement.**  
1251 File: Animation\_keops2bloom2011\_2012.mp4  
1252 The animation shows a full annual cycle of phytoplankton bloom development over and  
1253 downstream of the Kerguelen plateau from daily 8km resolution NASA MODIS Aqua  
1254 chlorophyll images. The images were provided by SSALTO/DUACS at CLS with support  
1255 from the Centre Nationale des Etudes Spatiales, Toulouse, France.  
1256  
1257 *Acknowledgements.* The Institute Polaire Paul-Emile Victor, the captain and crew of the  
1258 *Marion Dufresne*, the Australian Commonwealth Cooperative Research Centre Program,  
1259 and CSIRO Marine and Atmospheric Research (CMAR) provided logistic and financial  
1260 support. Special thanks to Pierre Sangiardi (IPEV) for implementing the underway  
1261 seawater supply for our high volume particle sampling and underway sensor mapping;  
1262 Louise Oriole (Laboratoire d’Océanographie Microbienne, Banyuls sur mer, France) for  
1263 shipboard nutrient analyses; Abraham Passmore (ACE CRC) for BSi analyses; Peter  
1264 Jansen (IMOS) for the logging system for the underway ISUS ultra-violet nitrate sensor;  
1265 Ben Weeding (IMOS) for advancing ISUS calibration; Thomas Rodemann for CHN  
1266 analyses in the University of Tasmania Central Sciences Laboratory; VUB for nitrate  
1267 isotope analyses, Clair Lo Monaco and Nicolas Metzl (LOCEAN, UPMC-CNRS) for  
1268 access to  $p\text{CO}_2$  results; and Andy Bowie (ACE CRC/UTAS), Pier van der Merwe (ACE  
1269 CRC), and Fabien Queroue (UTAS/UBO) for access to iron results. This work was  
1270 supported by the French Research program of INSU-CNRS LEFE–CYBER (Les  
1271 enveloppes fluides et l’environnement –Cycles biogéochimiques, environnement et  
1272 ressources), the French ANR (Agence Nationale de la Recherche, SIMI-6 program, ANR-  
1273 10-BLAN-0614), and the French CNES (Centre National d’Etudes Spatiales).

1274 **References**

- 1275 Anderson, L., and Sarmiento, J.: Redfield ratios of remineralization determined by nutrient  
1276 data analysis, *Global Biogeochemical Cycles*, 8, 65– 80, 1994.
- 1277 Armstrong, R. A.: An optimization-based model of iron-light-ammonium colimitation of  
1278 nitrate uptake and phytoplankton growth, *Limnology and Oceanography*, 44, 1436-1446,  
1279 1999.
- 1280 Arrigo, K. R., Robinson, D. H., Worthen, D. L., Dunbar, R. B., DiTullio, G. R., VanWoert,  
1281 M., and Lizotte, M. P.: Phytoplankton community structure and the drawdown of nutrients  
1282 and CO<sub>2</sub> in the Southern Ocean, *Science*, 283, 365-367, 1999.
- 1283 Assmy, P., Smetacek, V., Montresor, M., Klaas, C., Henjes, J., Strass, V. H., Arrieta, J. M.,  
1284 Bathmann, U., Berg, G. M., and Breitbarth, E.: Thick-shelled, grazer-protected diatoms  
1285 decouple ocean carbon and silicon cycles in the iron-limited Antarctic Circumpolar  
1286 Current, *Proceedings of the National Academy of Sciences*, 110, 20633-20638, 2013.
- 1287 Avak, H., and Fry, B.: EA-IRMS: Precise and accurate measurement of d15N on <10ug N,  
1288 Finnigan MAT Application flash report G29, 1-4, 1999.
- 1289 Blain, S., Queguiner, B., and Trull, T.: The natural iron fertilization experiment KEOPS  
1290 (KErguelen Ocean and Plateau compared Study): An overview, *Deep-Sea Research Part*  
1291 *II-Topical Studies in Oceanography*, 55, 559-565, 10.1016/j.dsr2.2008.01.002, 2008.
- 1292 Blain, S., Capparos, J., Guéneuguès, A., Obernosterer, I., and Oriol, L.: Distributions and  
1293 stoichiometry of dissolved nitrogen and phosphorus in the iron fertilized region near  
1294 Kerguelen (Southern Ocean), *Biogeosciences Discuss.*, 11, 9949-9977, 10.5194/bgd-11-  
1295 9949-2014, 2014.
- 1296 Bowie, A., van der Merwe, P., Trull, T., Queroue, F., Fourquez, M., Planchon, F., Sarthou,  
1297 G., and Blain, S.: Iron budgets for three distinct biogeochemical sites around the  
1298 Kerguelen plateau (Southern Ocean) during the natural fertilization experiment KEOPS-2,  
1299 *Biogeosciences Discuss.*, 11, submitted, 2014.
- 1300 Boyd, P., Watson, A., Law, C. S., Abraham, E., Trull, T., and Murdoch, R.: SOIREE - A  
1301 Southern Ocean iron release experiment elevates phytoplankton stocks in Polar waters.,  
1302 *EOS Trans. AGU Ocean Sciences Meet. Suppl.*, 80, OS30, 1999.
- 1303 Boyd, P. W., and Newton, P.: Evidence of the potential influence of planktonic  
1304 community structure on the interannual variability of particulate carbon flux., *Deep-Sea*  
1305 *Research I*, 42, 619-639, 1995.
- 1306 Boyd, P. W., and Newton, P.: Does planktonic community structure determine downward  
1307 particulate organic carbon flux in different oceanic provinces?, *Deep-Sea Research I*, 46,  
1308 63-91, 1999.
- 1309 Boyd, P. W., Jickells, T., C. S. Law, Blain, S., Boyle, E. A., Buesseler, K. O., Coale, K. H.,  
1310 Cullen, J. J., Baar, H. J. W. d., Follows, M., Harvey, M., Lancelot, C., Levasseur, M.,  
1311 Owens, N. P. J., Pollard, R., Rivkin, R. B., Sarmiento, J., Schoemann, V., Smetacek, V.,  
1312 Takeda, S., Tsuda, A., Turner, S., and Watson, A. J.: Mesoscale Iron Enrichment  
1313 Experiments 1993-2005: Synthesis and Future Directions, *Science*, 315, 612 - 617, DOI:  
1314 610.1126/science.1131669, 2007.
- 1315 Boyd, P. W., and Trull, T. W.: Understanding the export of marine biogenic particles: is  
1316 there consensus?, *Progress in Oceanography*, 4, 276-312,  
1317 doi:210.1016/j.pocean.2006.1010.1007, 2007.
- 1318 Brooks, P. D., Geilmann, H., Werner, R. A., and Brand, W. A.: Improved precision of  
1319 coupled 13C and 15N measurements from single samples using an elemental analyser,  
1320 *Rapid Communications in Mass Spectroscopy*, 17, 1924-1926, 2003.
- 1321 Buesseler, K. O.: The decoupling of production and particulate export in the surface ocean,  
1322 *Global Biogeochemical Cycles*, 12, 297-310, 1998.

1323 Buesseler, K. O., Ball, L., Andrews, J. E., Cochran, J. K., Hirschberg, D. J., Bacon, M. P.,  
1324 Fleer, A., and Brzezinski, M.: Upper ocean export of particulate organic carbon and  
1325 biogenic silica in the Southern Ocean along 170°W, *Deep-Sea Research II*, 48, 4275–4297,  
1326 2001.

1327 Buesseler, K. O., Lamborg, C. H., Boyd, P. W., Lam, P. J., Trull, T. W., Bidigare, R. R.,  
1328 Bishop, J. K. B., Casciotti, K. L., Dehairs, F., Elskens, M., Honda, M., Karl, D. M., Siegel,  
1329 D., Silver, M., Steinberg, D., Valdes, J., Van Mooy, B., and Wilson, S. E.: Revisiting  
1330 carbon flux through the Ocean's twilight zone, *Science*, 316, 567 - 570, DOI:  
1331 510.1126/science.1137959, 2007.

1332 Burkhardt, S., Riebesell, U., and Zondervan, I.: Effects of growth rate, CO<sub>2</sub> concentration,  
1333 and cell size on the stable carbon isotope fractionation in marine phytoplankton,  
1334 *Geochimica et Cosmochimica Acta*, 63, 3729-3741, 1999a.

1335 Burkhardt, S., Riebesell, U., and Zondervan, I.: Effects of growth rate, CO<sub>2</sub> concentration,  
1336 and cell size on the stable carbon isotope fractionation in marine phytoplankton,  
1337 *Geochimica Cosmochimica Acta*, 63, 3729-3741, 1999b.

1338 Burkhardt, S., Riebesell, U., and Zondervan, I.: Stable carbon isotope fractionation by  
1339 marine phytoplankton in response to daylength, growth rate, and CO<sub>2</sub> availability, *Marine*  
1340 *ecology-progress series*, 184, 31-41, 1999c.

1341 Carlotti, F., Jouandet, M.-P., Nowaczyk, A., Harmelin-Vivien, M., Lefèvre, D., Guillou,  
1342 G., Zhu, Y., and Zhou, M.: Mesozooplankton structure and functioning during the onset of  
1343 the Kerguelen Bloom during Keops2 survey., *Biogeosciences Discuss.*, 11, submitted,  
1344 2014.

1345 Cavagna, A.-J., Fripiat, F., Elskens, M., Dehairs, F., Mangion, P., Chirurgien, I., Closset,  
1346 I., Lasbleiz, M., Flores-Leive, L., Cardinal, D., Leblanc, K., Fernandez, C., Lefevre, D.,  
1347 Oriol, L., and Queguiner, B.: Biological productivity regime in the surface water around  
1348 the Kerguelen Island area, *Southern Ocean.*, *Biogeosciences Discuss.*, 11, submitted,  
1349 2014.

1350 Chisholm, S. W.: Phytoplankton size, in: *Primary productivity and biogeochemical cycles*  
1351 *in the sea*, edited by: Falkowski, P., and Woodhead, A., Environmental Science Research,  
1352 Springer, 213-237, 1992.

1353 Christaki, U., Lefèvre, D., Georges, C., Colombet, J., Catala, P., Courties, C., Sime-  
1354 Ngando, T., Blain, S., and Obernosterer, I.: Microbial food web dynamics during spring  
1355 phytoplankton blooms in the naturally iron-fertilized Kerguelen area (Southern Ocean),  
1356 *Biogeosciences Discuss.*, 11, 6985-7028, 10.5194/bgd-11-6985-2014, 2014.

1357 Cózar, A., and Echevarría, F.: Size structure of the planktonic community in microcosms  
1358 with different levels of turbulence, *Scientia Marina*, 69, 187-197, 2005.

1359 Craig, H.: The geochemistry of the stable carbon isotopes, *Geochimica et Cosmochimica*  
1360 *Acta*, 3, 53-92, 1953.

1361 Cullen, J. J.: Status of the iron hypothesis after the Open-Ocean Enrichment Experiment,  
1362 *Limnology and Oceanography*, 40, 1336-1343, 1995.

1363 d'Ovidio, F., Della Penna, A., Trull, T. W., Nencioli, I., Pujol, I., Rio, M. H., Park, Y.-H.,  
1364 Cotte, C., Zhou, M., and Blain, S.: The biogeochemical structuring role of horizontal  
1365 stirring: Lagrangian perspectives on iron delivery downstream of the Kerguelen plateau,  
1366 *Biogeosciences Discussions*, 11, submitted, 2014.

1367 de Baar, H. J. W., de Jong, J. T. M., Bakker, D. C. E., Loscher, B. M., Veth, C., Bathmann,  
1368 U., and Smetacek, V.: Importance of iron for phytoplankton blooms and carbon dioxide  
1369 drawdown in the Southern Ocean, *Nature*, 373, 412-415, 1995.

1370 Dehairs, F., Fripiat, F., Cavagna, A. J., Trull, T. W., Fernandez, C., Davies, D., Roukaerts,  
1371 A., Fonseca Batista, D., Planchon, F., and Elskens, M.: Nitrogen cycling in the Southern  
1372 Ocean Kerguelen Plateau area: evidence for significant surface nitrification from nitrate

1373 isotopic compositions, *Biogeosciences Discuss.*, 11, 13905-13955, 10.5194/bgd-11-  
1374 13905-2014, 2014.

1375 Farquhar, G. D., O'Leary, M. H., and Berry, J. A.: On the relationship between carbon  
1376 isotope discrimination and the intracellular carbon dioxide concentration in leaves,  
1377 *Australian Journal of Plant Physiology*, 9, 121-137, 1982.

1378 Fontugne, M., Descolas-Gros, C., and de Billy, G.: The dynamics of CO<sub>2</sub> fixation in the  
1379 Southern Ocean as indicated by carboxylase activities and organic carbon isotope ratios,  
1380 *Marine Chemistry*, 35, 371-380, 1991.

1381 Georges, C., Monchy, S., Genitsaris, S., and Christaki, U.: Protist community composition  
1382 during early phytoplankton blooms in the naturally iron-fertilized Kerguelen area  
1383 (Southern Ocean), *Biogeosciences Discuss.*, 11, 11179-11215, 10.5194/bgd-11-11179-  
1384 2014, 2014.

1385 Gervais, F., and Riebesell, U.: Effect of phosphorus limitation on elemental composition  
1386 and stable carbon isotope fractionation in a marine diatoms growing under different CO<sub>2</sub>  
1387 concentrations., *Limnology and Oceanography*, 46, 497-504, 2001.

1388 Goericke, R., Montoya, J. P., and Fry, B.: Physiology of isotopic fractionation in algae and  
1389 cyanobacteria, in: *Stable Isotopes in Ecology and Environmental Science*, edited by:  
1390 Lajtha, K., and Michener, R. H., Blackwell Scientific Publications, Oxford, 1870-1221,  
1391 1994.

1392 Hoffman, L. J., Peeken, I., and Lochte, K.: Effects of iron on the elemental stoichiometry  
1393 during EIFEX and in the diatoms *Fragilariopsis kerguelensis* and *Chaetoceros dichaeta*,  
1394 *Biogeosciences*, 4, 569-579, 2007.

1395 Hutchins, D. A., and Bruland, K. W.: Iron limited diatom growth and Si:N uptake ratios in  
1396 a coastal upwelling regime, *Nature*, 393, 561-564, 1998.

1397 Jacquet, S. H. M., Dehairs, F., Cavagna, A. J., Planchon, F., Monin, L., André, L., Closset,  
1398 I., and Cardinal, D.: Early season mesopelagic carbon remineralization and transfer  
1399 efficiency in the naturally iron-fertilized Kerguelen area, *Biogeosciences Discuss.*, 11,  
1400 9035-9069, 10.5194/bgd-11-9035-2014, 2014.

1401 Karsh, K. L., Trull, T. W., Lourey, A. J., and Sigman, D. M.: Relationship of nitrogen  
1402 isotope fractionation to phytoplankton size and iron availability during the Southern Ocean  
1403 Iron Release Experiment (SOIREE), *Limnology and Oceanography*, 48, 1058-1068, 2003.

1404 Karsh, K. L., Trull, T. W., Sigman, D. M., Thompson, P. A., and Granger, J.: The  
1405 contributions of nitrate uptake and efflux to isotope fractionation during algal nitrate  
1406 assimilation, *Geochimica et Cosmochimica Acta*, 132, 391-412,  
1407 <http://dx.doi.org/10.1016/j.gca.2013.09.030>, 2014.

1408 Keller, K., and Morel, F. M. M.: A model of carbon isotopic fractionation and active  
1409 carbon uptake in phytoplankton, *Marine Ecology-Progress Series*, 182, 295-298, 1999.

1410 King, P., Kennedy, H., Newton, P., Jickells, T., Brand, T., Calvert, S., Cauwet, G.,  
1411 Etcheber, H., Head, B., Khrifpounoff, A., Manighetti, B., and Miquel, J. C.: Analysis of  
1412 total and organic carbon and total nitrogen in settling oceanic particles and marine  
1413 sediment: an interlaboratory comparison, *Marine Chemistry*, 60, 203-216, 1998.

1414 Lasbleiz, M., Leblanc, K., Blain, S., Ras, J., Cornet-Barthaux, V., Hélias Nunige, S., and  
1415 Quéguiner, B.: Pigments, elemental composition (C, N, P, Si) and stoichiometry of  
1416 particulate matter, in the naturally iron fertilized region of Kerguelen in the Southern  
1417 Ocean, *Biogeosciences Discuss.*, 11, 8259-8324, 10.5194/bgd-11-8259-2014, 2014.

1418 Laurenceau, E. C., Trull, T. W., Davies, D. M., Bray, S. G., Doran, J., Planchon, F.,  
1419 Carlotti, F., Jouandet, M. P., Cavagna, A. J., Waite, A. M., and Blain, S.: The relative  
1420 importance of phytoplankton aggregates and zooplankton fecal pellets to carbon export:  
1421 insights from free-drifting sediment trap deployments in naturally iron-fertilised waters

1422 near the Kerguelen plateau, *Biogeosciences Discuss.*, 11, 13623-13673, 10.5194/bgd-11-  
1423 13623-2014, 2014.

1424 Laws, E. A., Popp, B. N., Bidigare, R. R., Kennicutt, M. C., and Macko, S. A.:  
1425 Dependence of phytoplankton carbon isotopic composition on growth rate and  $[CO_2]_{aq}$ :  
1426 Theoretical considerations and experimental results, *Geochimica et Cosmochimica Acta*,  
1427 59, 1131-1138, 1995.

1428 Laws, E. A., Popp, B. N., Cassar, N., and Tanimoto, J.:  $^{13}C$  discrimination patterns in  
1429 oceanic phytoplankton: likely influence of  $CO_2$  concentrating mechanisms, and  
1430 implications for palaeoreconstructions, *Functional Plant Biology*, 29, 323-333, 2002.

1431 Leynaert, A., Bucciarelli, E., Claquin, P., Dugdale, R. C., Martin-Jézéquel, V., Pondaven,  
1432 P., and Ragueneau, O.: Effect of iron deficiency on diatom cell size and silicic acid uptake  
1433 kinetics, *Limnology and Oceanography*, 49, 1134-1143, 2004.

1434 Lo Monaco, C., Metzl, N., D'Ovidio, F., Llorca, J., and Ridame, C.: Rapid establishment of  
1435 the  $CO_2$  sink associated with Kerguelen's bloom observed during the KEOPS2/OISO20  
1436 cruise, *Biogeosciences Discuss.*, 11, in preparation, 2014.

1437 Maldonado, M. T., Boyd, P. W., Abraham, E., Bowie, A., Croot, P., Strzepek, R., Waite,  
1438 A., LaRoche, J., Frew, R., and Price, N.: Iron uptake and physiological response of  
1439 phytoplankton during a mesoscale Southern Ocean Iron enrichment, *Limnology and*  
1440 *oceanography*, 46, 1802-1808, 2001.

1441 Marchetti, A., and Cassar, N.: Diatom elemental and morphological changes in response to  
1442 iron limitation: a brief review with potential paleoceanographic applications, *Geobiology*,  
1443 7, 419-431, 2009.

1444 Michener, R. H., and Schell, D. M.: Stable isotope ratios as tracers in marine aquatic food  
1445 webs, in: *Stable isotopes in ecology and environmental science*, edited by: Lajtha, K., and  
1446 Michener, R. H., Blackwell Scientific Publications, Oxford, 138-157, 1994.

1447 Morel, F. M. M., Reuter, J. G., and Price, N. M.: Iron nutrition of phytoplankton and its  
1448 possible importance in the ecology of ocean regions with high nutrient and low biomass,  
1449 *Oceanography*, 4, 56-61, 1991.

1450 Mosseri, J., Quéguiner, B., Armand, L., and Cornet-Barthaux, V.: Impact of iron on silicon  
1451 utilization by diatoms in the Southern Ocean: a case study of the Si/N cycle decoupling in  
1452 a naturally iron-enriched area, *Deep Sea Research II*, 55, 801-819, 2008.

1453 Park, Y.-H., Roquet, F., Fuda, J.-L., and Durand, I.: Large scale circulation over and  
1454 around the Kerguelen Plateau, *Deep Sea Research II*, 55, 566-581, 2008.

1455 Park, Y.-H., Durand, I., Kestenare, E., Rougier, G., Zhou, M., d'Ovidio, F., Cotté, C., and  
1456 Lee, J.-H.: Polar Front around the Kerguelen Islands: An up-to-date determination and  
1457 associated circulation of surface/subsurface waters, *Journal of Geophysical Research:*  
1458 *Oceans*, 2169-9291, DOI: 10.1002/2014JC010061, 2014a.

1459 Park, Y. H., Lee, J. H., Durand, I., and Hong, C. S.: Validation of the Thorpe scale-derived  
1460 vertical diffusivities against microstructure measurements in the Kerguelen region,  
1461 *Biogeosciences Discuss.*, 11, 12137-12157, 10.5194/bgd-11-12137-2014, 2014b.

1462 Planchon, F., Ballas, D., Cavagna, A.-J., Bowie, A., Davies, D., Trull, T., Laurenceau, E.,  
1463 van der Merwe, P., and Dehairs, F.: Carbon export in the naturally iron-fertilized  
1464 Kerguelen area of the Southern Ocean based on the  $^{234}Th$  approach, *Biogeosciences*  
1465 *Discuss.*, 11, submitted, 2014.

1466 Pollard, R., Sanders, R., Lucas, M., and Statham, P.: The Crozet Natural Iron Bloom and  
1467 Export Experiment (CROZEX), *Deep-Sea Research II*, Volume 54, Issue 18-20, p. , 54,  
1468 1905-1914, 2007.

1469 Popp, B. N., Kenig, F., Wakeham, S. G., Laws, E. A., and Bidigare, R. R.: Does growth  
1470 rate affect ketone unsaturation and intracellular carbon isotopic variability in *Emiliana*  
1471 *huxleyi*?, *Paleoceanography*, 13, 35-41, 1998a.

1472 Popp, B. N., Laws, E. A., Bidigare, R. R., Dore, J. E., Hanson, K. L., and Wakeham, S. G.:  
1473 Effect of phytoplankton cell geometry on carbon isotopic fractionation, *Geochimica et*  
1474 *Cosmochimica Acta*, 62, 69-77, 1998b.

1475 Popp, B. N., Trull, T., Kenig, F., Wakeham, S. G., Rust, T. M., Tilbrook, B., Griffiths, F.  
1476 B., Wright, S. W., Marchant, H. J., Bidigare, R. R., and Laws, E. A.: Controls on the  
1477 carbon isotopic composition of Southern Ocean phytoplankton, *Global Biogeochemical*  
1478 *Cycles*, 13, 827-843, 1999.

1479 Queguiner, B.: Biogenic silica production in the Australian sector of the Subantarctic Zone  
1480 of the Southern Ocean in late summer 1998, *Journal of Geophysical Research*, 106, 31627-  
1481 31636, 2001.

1482 Queguiner, B.: Iron fertilization and the structure of planktonic communities in high  
1483 nutrient regions of the Southern Ocean, *Deep Sea Research II*, 90, 43-54, 2013.

1484 Quéroué, F., Sarthou, G., Planquette, H. F., Bucciarelli, E., Chever, F., van der Merwe, P.,  
1485 Lannuzel, D., Townsend, A., Cheize, M., Blain, S., d'Ovidio, F., and Bowie, A. R.: High  
1486 variability of dissolved iron concentrations in the vicinity of Kerguelen Island (Southern  
1487 Ocean), *Biogeosciences Discuss.*, 11, submitted, 2014.

1488 Ragueneau, O., Schultes, S., Bidle, K., Claquin, P., and Moriceau, B.: Si and C  
1489 interactions in the world ocean: Importance of ecological processes and implications for  
1490 the role of diatoms in the biological pump, *Global Biogeochemical Cycles*, 20, GB4S02,  
1491 2006.

1492 Rau, G. H., Teyssie, J.-L., Rassoulzadegan, F., and Fowler, S. W.:  $^{13}\text{C}/^{12}\text{C}$  and  $^{15}\text{N}/^{14}\text{N}$   
1493 variations among size fractionated marine particles: implications for their origin and  
1494 trophic relationships., *Marine Ecology Progress Series*, 59, 33-38, 1990.

1495 Rau, G. H., Riebesell, U., and Wolf-Gladrow, D.: A model of photosynthetic  $^{13}\text{C}$   
1496 fractionation by marine phytoplankton based on diffusive molecular  $\text{CO}_2$  uptake, *Marine*  
1497 *Ecology Progress Series*, 133, 275-285, 1996.

1498 Rau, G. H., Riebesell, U., and Wolf-Gladrow, D.:  $\text{CO}_{2\text{aq}}$ -dependent photosynthetic  $^{13}\text{C}$   
1499 fractionation in the ocean: A model versus measurements, *Global Biogeochemical Cycles*,  
1500 11, 267-278, 1997.

1501 Redfield, A. C., Ketchum, B. H., and Richards, F. H.: The influence of organisms on the  
1502 composition of seawater, in: *The Sea*, edited by: Hill, M. N., Inter-Science, New York, 26-  
1503 77, 1963.

1504 Sanial, V., van Beek, P., Lansard, B., Souhaut, M., Kestenare, E., d'Ovidio, F., Zhou, M.,  
1505 and Blain, S.: Use of Ra isotopes to deduce rapid transfer of sediment-derived inputs off  
1506 Kerguelen, *Biogeosciences Discuss.*, 11, 14023-14061, 10.5194/bgd-11-14023-2014, 2014.

1507 Savoye, N., Trull, T. W., Jacquet, S. H. M., Navez, J., and Dehairs, F.: Th-234-based  
1508 export fluxes during a natural iron fertilization experiment in the Southern Ocean  
1509 (KEOPS), *Deep-Sea Research Part II-Topical Studies in Oceanography*, 55, 841-855,  
1510 10.1016/j.dsr2.2007.12.036, 2008.

1511 Schulz, K. G., Zondervan, I., Gerringa, L. J. A., Timmermans, K. R., Veldhuis, M. J. W.,  
1512 and Riebesell, U.: Effect of trace metal availability on coccolithophorid calcification,  
1513 *Nature*, 430, 673-676, 2004.

1514 Schulz, K. G., Rost, B., Burkhardt, S., Riebesell, U., Thoms, S., and Wolf-Gladrow, D.:  
1515 The effect of iron availability on the regulation of inorganic carbon acquisition in the  
1516 coccolithophore *Emiliania huxleyi* and the significance of cellular compartmentation for  
1517 stable carbon isotope fractionation, *Geochimica et Cosmochimica Acta*, 71, 5301-5312,  
1518 2007.

1519 Smetacek, V.: Role of sinking in diatom life-history cycles: ecological, evolutionary and  
1520 geological significance, *Marine Biology*, 84, 239-251, 1985.

1521 Smetack, V.: Diatoms and the silicate factor, *Nature*, 391, 224-225, 1998.

1522 Sokolov, S., and Rintoul, S. R.: Circumpolar structure and distribution of the Antarctic  
1523 Circumpolar Current fronts: 1. Mean circumpolar paths, *Journal of geophysical research*,  
1524 114, C11018, 2009.

1525 Sweeney, C., Hansell, D. A., Carlson, C. A., Codispoti, L. A., Gordon, L. I., Marra, J.,  
1526 Millero, F. J., Smith, W. O., and Takahashi, T.: Biogeochemical regimes, net community  
1527 production and carbon export in the Ross Sea, Antarctica, *Deep-Sea Research II*, 47, 3369-  
1528 3394, 2000.

1529 Syvaranta, J., and Rautio, M.: Zooplankton, lipids and stable isotopes: importance of  
1530 seasonal, latitudinal, and taxonomic differences, *Canadian Journal of Fisheries and*  
1531 *Aquatic Sciences*, 67, 1721-1729, 2010.

1532 Takeda, S.: Influence of iron availability on nutrient consumption ratio of diatoms in  
1533 oceanic waters, *Nature*, 393, 774-777, 1998.

1534 Tortell, P. D., Payne, C., Gueguen, C., Li, Y., Strzepek, R., Boyd, P., and Rost, B.: Uptake  
1535 and assimilation of inorganic carbon by Southern Ocean phytoplankton, *Limnology and*  
1536 *Oceanography*, 53 (4) 1278., 53, 1266-1278, 2008.

1537 Tremblay, 2014.

1538 Trull, T. W., and Armand, L.: Insights into Southern Ocean carbon export from the delta  
1539 C-13 of particles and dissolved inorganic carbon during the SOIREE iron release  
1540 experiment, *Deep-Sea Research Part II-Topical Studies in Oceanography*, 48, 2655-2680,  
1541 10.1016/s0967-0645(01)00013-3, 2001.

1542 Trull, T. W., Davies, D., and Casciotti, K.: Insights into nutrient assimilation and export in  
1543 naturally iron-fertilized waters of the Southern Ocean from nitrogen, carbon and oxygen  
1544 isotopes, *Deep-Sea Research Part II-Topical Studies in Oceanography*, 55, 820-840,  
1545 10.1016/j.dsr2.2007.12.035, 2008.

1546 van der Merwe, P., Bowie, A. R., Qu  rou  , F., Armand, L., Blain, S., Chever, F., Davies,  
1547 D., Dehairs, F., Planchon, F., Sarthou, G., Townsend, A. T., and Trull, T.: Sourcing the  
1548 iron in the naturally-fertilised bloom around the Kerguelen Plateau: particulate trace metal  
1549 dynamics, *Biogeosciences Discuss.*, 11, 13389-13432, 10.5194/bgd-11-13389-2014, 2014.

1550 Wada, E., and Hattori, A.: Nitrogen isotope effects in the assimilation of inorganic  
1551 nitrogenous compounds by marine diatoms., *Geomicrobiology Journal*, 1, 85-101, 1978.

1552 Wang, X., Mearns, R. J., and Trull, T. W.: Nutrient utilization ratios in the Polar Frontal  
1553 Zone in the Australian sector of the Southern Ocean: a model, *Global Biogeochemical*  
1554 *Cycles*, 17, 1009, doi:10.1029/2002GB001938, 2003.

1555 Weiss, R. F.: Carbon dioxide in water and seawater: the solubility of a non-ideal gas,  
1556 *Marine Chemistry*, 2, 203-215, 1974.

1557 |

